Adipocyte REVERBα dictates adipose tissue expansion during obesity

A. Louise Hunter[1,5], Charlotte E. Pelekanou[1,5], Nichola J. Barron[1], Rebecca C. Northeast[1], Antony Adamson[1], Polly Downton[1], Thomas Cornfield[2], Peter S. Cunningham[1], Leanne Hodson[2], Andrew S.I. Loudon[1], Richard D. Unwin[3], Mudassar Iqbal[4], David W. Ray[2], David A. Bechtold[1]

1. Centre for Biological Timing, Faculty of Biology, Medicine and Health, University of Manchester
2. Oxford Centre for Diabetes, Endocrinology and Metabolism, University of Oxford, and NIHR Oxford Biomedical Research Centre, John Radcliffe Hospital
3. Stoller Biomarker Discovery Centre, Division of Cancer Sciences, Faculty of Biology, Medicine and Health, University of Manchester
4. Division of Informatics, Imaging & Data Sciences, Faculty of Biology, Medicine and Health, University of Manchester
5. These authors contributed equally

Correspondence:

David A. Bechtold, 3.002 AV Hill Building, University of Manchester, Manchester, M13 9PT, UK; David.Bechtold@manchester.ac.uk, Tel: +44(0)161 2755721

Keywords: Circadian clock, energy metabolism, obesity, metabolic disease, adipose, nuclear hormone receptor, NR1D1, extracellular matrix

ABSTRACT

The circadian clock component REVERBα is considered a dominant regulator of lipid metabolism, with global *Reverbα* deletion driving dysregulation of white adipose tissue (WAT) lipogenesis and obesity. However, a similar phenotype is not observed under adipocyte-selective deletion (*Reverbα*$^{Flox2\text{-}6}$*Adipo*^{Cre}), and transcriptional profiling demonstrates that, under basal conditions, direct targets of REVERBα regulation are limited, and include the circadian clock and collagen dynamics. Under high-fat diet (HFD) feeding, *Reverbα*$^{Flox2\text{-}6}$*Adipo*^{Cre} mice do manifest profound obesity, yet without the accompanying WAT inflammation and fibrosis exhibited by controls. Integration of the WAT REVERBα cistrome with differential gene expression reveals broad control of metabolic processes by REVERBα which is unmasked in the obese state. Adipocyte REVERBα does not drive an anticipatory daily rhythm in WAT lipogenesis, but rather modulates WAT activity in response to alterations in metabolic state. Importantly, REVERBα action in adipocytes is critical to the development of obesity-related WAT pathology and insulin resistance.

INTRODUCTION

The mammalian circadian clock directs rhythms in behaviour and physiology to coordinate our biology with predictable changes in food availability and daily alternations between fasted and fed states. In this way, profound cycles in nutrient availability and internal energy state can be managed across multiple organ systems. A central circadian clock in the suprachiasmatic nuclei (SCN) drives daily rhythms in our behaviour (e.g. sleep/wake cycles) and physiology (e.g. body temperature), and orchestrates rhythmic processes in tissue systems across the body (Dibner et al., 2010; West and Bechtold, 2015). The molecular clock mechanism is also present in most cells and tissue. Normal peripheral tissue function and expression of a 'complete' rhythmic transcriptome requires local tissue clock activity, as well as input from the central clock and rhythmic systemic signals (Guo et al., 2005; Hughes et al., 2012; Kornmann et al., 2007; Koronowski et al., 2019; Lamia et al., 2008). The relative importance of each of these factors remains ill-defined. Nevertheless, it is clear that our rhythmic physiology and metabolic status reflects the interaction of clocks across the brain and body (West and Bechtold, 2015). Disturbance of this interaction, as occurs with shift work and irregular eating patterns, is increasingly recognised as a risk factor for metabolic disease and obesity (Broussard and Cauter, 2016; Kim et al., 2019).

Extensive work over the past 20 years has demonstrated that circadian clock function and its component factors are closely tied into energy metabolism (Bass and Takahashi, 2010; Reinke and Asher, 2019), with strong rhythmicity evident in cellular and systemic metabolic processes. Clock-metabolic coupling in peripheral tissues is adaptable, as demonstrated by classical food-entrainment studies (Damiola et al., 2000; Mistlberger, 1994), and by recent work showing that systemic perturbations such as cancer and high-fat diet feeding can re-programme circadian control over liver metabolism (Dyar et al., 2018; Masri et al., 2016). Plasticity therefore exists within the system, and the role of the clock in tissue and systemic responses to acute and chronic metabolic perturbation remains a critical question. The nuclear

receptor REVERBα (NR1D1) is a core clock component, and has been highlighted as a key link between the clock and metabolism. REVERBα is a constitutive repressor, with peak expression in the latter half of the inactive phase (daytime in the nocturnal animal). In liver, REVERBα exerts repressive control over programmes of lipogenesis by recruiting the NCOR/HDAC3 co-repressor complex to metabolic target genes, such that loss of REVERBα or HDAC3 results in hepatosteatosis (Feng et al., 2011; Zhang et al., 2016, 2015). The selective functions of REVERBα in white adipose tissue (WAT) are not well-established and remain poorly understood. Early studies implicated an essential role of *Reverba* in adipocyte differentiation (Chawla and Lazar, 1993; Kumar et al., 2010); however, these findings are difficult to align with *in vivo* evidence. Indeed, pronounced adiposity and adipocyte hypertrophy are evident in *Reverbα*$^{-/-}$ mice, even under normal feeding conditions (Delezie et al., 2012; Hand et al., 2015; Zhang et al., 2015). Moreover, daily administration of REVERBα agonists has been shown to reduce fat mass and WAT lipogenic gene expression in mice (Solt et al., 2012), despite concerns about off-targets actions of these agents (Dierickx et al., 2019). Given the links between circadian disruption and obesity, and the potential of REVERBα as a pharmacological target, we now define the role of REVERBα in dictating WAT metabolism.

Transcriptomic and proteomic profiling of WAT in global *Reverbα*$^{-/-}$ mice revealed an expected de-repression of lipid synthesis and storage programmes. However, in contrast, selective deletion of *Reverbα* in adipocytes did not result in dysregulation of WAT metabolic pathways. Loss of REVERBα activity in WAT did, however, significantly enhance adipose tissue expansion in response to HFD feeding; yet despite the exaggerated obesity, adipocyte-specific knockout mice were spared anticipated obesity-related pathology. Integration of transcriptomic data with the WAT REVERBα cistrome demonstrates that, under basal conditions, REVERBα activity is limited to a small set of direct target genes (enriched for extracellular matrix processes). However, REVERBα-regulatory control broadens to include lipid and mitochondrial metabolism pathways under conditions of obesity. Our data recast the role of

94 REVERBα as a regulator responsive to the metabolic state of the tissue, rather than one which
95 delivers an anticipatory daily oscillation to the WAT metabolic programme.

RESULTS

Adiposity and up-regulation of WAT lipogenic pathways in *Reverbα*$^{-/-}$ mice

We first examined the body composition of age-matched *Reverbα* global knockout (KO) (*Reverbα*$^{-/-}$) mice and littermate controls (WT). In keeping with previous reports (Delezie et al., 2012; Hand et al., 2015), *Reverbα*$^{-/-}$ mice are of similar body weight to littermate controls (**Figure 1A**), yet carry an increased proportion of fat mass (KO: 24.2 ±3.0% of body weight; WT: 10.8 ±1.4%; mean ±SEM, P<0.01 Student's t-test, n=12-14/group) and display adipocyte hypertrophy (**Figure 1B**), even when maintained on a standard chow diet. Metabolic phenotyping demonstrated expected day-night differences in food intake, energy expenditure, activity, and body temperature in both KO and WT controls, although genotype differences in day/night activity and temperature levels suggest some dampening of rhythmicity in the *Reverbα*$^{-/-}$ mice (**Figure 1 Supplemental A-E**). However, this is unlikely to account for the increased adiposity in these animals, and a previous study did not report significant genotype differences in these parameters (Delezie et al., 2012). This favours instead an altered energy partitioning within these mice, with a clear bias towards storing energy as lipid.

To explore further the lipid storage phenotype, we undertook proteomic analysis of gonadal white adipose tissue (gWAT) collected at ZT8 (*zeitgeber* time, 8h after lights on), the time of normal peak in REVERBα expression in this tissue (**Figure 1 Supplemental F**). Isobaric tag (iTRAQ) labelled LC-MS/MS identified 2257 proteins, of which 182 demonstrated differential regulation (FDR<0.05) between WT and *Reverbα*$^{-/-}$ gWAT samples (n=6 weight-matched, 13-week old male mice/group) (**Figure 1C**). Differentially expressed proteins included influential metabolic enzymes, with up-regulation of metabolic processes detected on pathway enrichment analysis (**Figure 1D**). Importantly, and in line with the phenotype observed, increased NADPH regeneration (e.g. ME1, G6PDX), enhancement of glucose metabolism, (also likely reflecting increased glyceroneogenesis; e.g. PFKL, ALDOA), and up-regulation of fatty acid synthesis (e.g. ACYL, FAS, ACACA) all support a shunt towards synthesis and

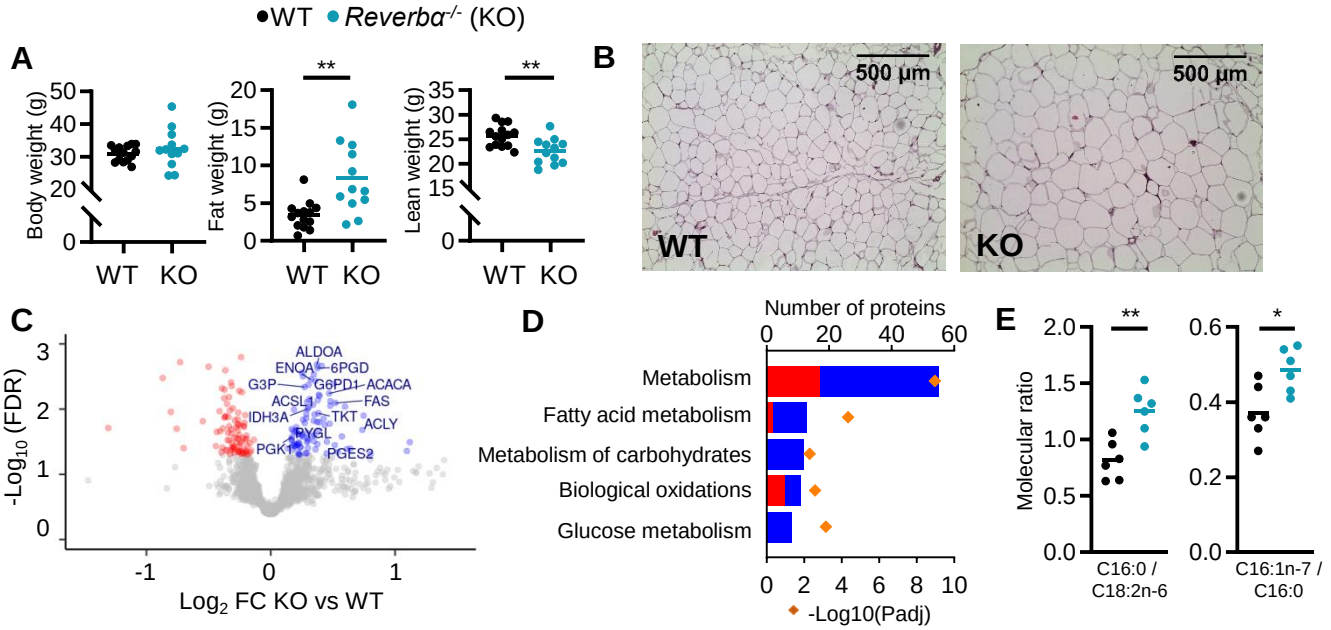

FIGURE 1. Global deletion of *Reverbα* results in obesity and increased adipose lipid synthesis.
A. *Reverbα*$^{-/-}$ mice exhibit significantly greater fat mass relative to WT littermate controls. Body weight, fat mass and lean mass of 13-week old males (n=12-14/group). **B**. Increased fat mass in *Reverbα*$^{-/-}$ mice is reflected in adipocyte hypertrophy in gonadal white adipose tissue (gWAT) (representative x10 H&E images shown). **C**,**D**. gWAT from *Reverbα*$^{-/-}$ mice exhibits a programme of increased lipid synthesis. Proteomic profiling of gWAT depots (*Reverbα*$^{-/-}$ mice plotted relative to their respective weight-matched littermate controls, n=6/group (**C**)) shows deregulation of metabolic regulators and enrichment (**D**) of metabolic pathways (up- and down-regulated proteins shown in blue and red respectively). Top five (by protein count) significantly enriched Reactome terms shown. **E**. Analyses of fatty acid (FA) composition reveal increased *de novo* lipogenesis (reflected by C16:0/C18:2n ratio) and FA desaturation (reflected by C16:1n-7/C16:0 ratio) in gWAT of *Reverbα*$^{-/-}$ mice. n=6/group.

Data presented as mean with individual data points (**A**, **E**). *P<0.05, **P<0.01, unpaired two-tailed t-test (**A**, **E**).

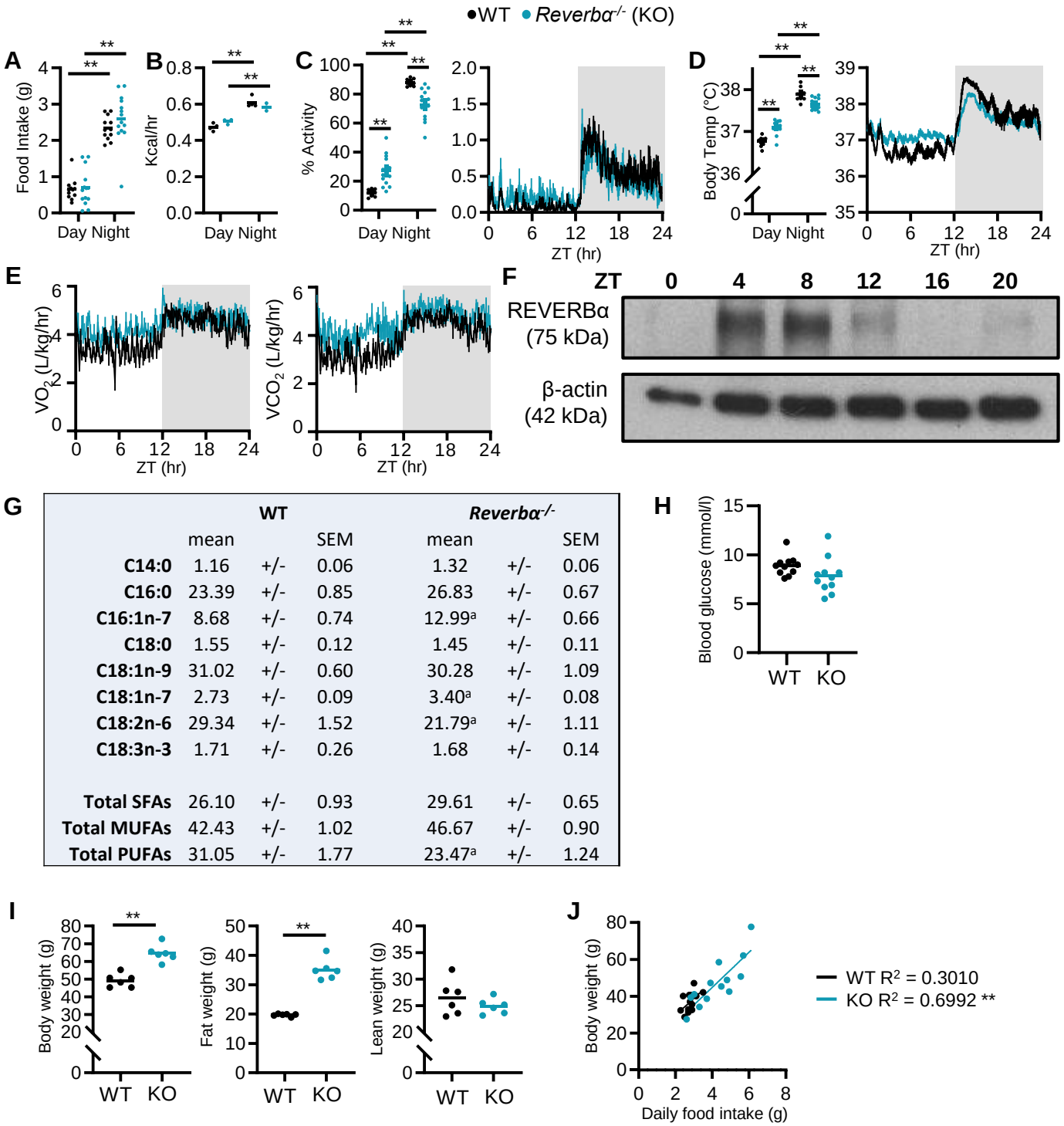

G

	WT			*Reverbα*$^{-/-}$		
	mean		SEM	mean		SEM
C14:0	1.16	+/-	0.06	1.32	+/-	0.06
C16:0	23.39	+/-	0.85	26.83	+/-	0.67
C16:1n-7	8.68	+/-	0.74	12.99[a]	+/-	0.66
C18:0	1.55	+/-	0.12	1.45	+/-	0.11
C18:1n-9	31.02	+/-	0.60	30.28	+/-	1.09
C18:1n-7	2.73	+/-	0.09	3.40[a]	+/-	0.08
C18:2n-6	29.34	+/-	1.52	21.79[a]	+/-	1.11
C18:3n-3	1.71	+/-	0.26	1.68	+/-	0.14
Total SFAs	26.10	+/-	0.93	29.61	+/-	0.65
Total MUFAs	42.43	+/-	1.02	46.67	+/-	0.90
Total PUFAs	31.05	+/-	1.77	23.47[a]	+/-	1.24

FIGURE 1 SUPPLEMENTAL. Rhythmic physiology and susceptibility to diet-induced obesity in *Reverbα*$^{-/-}$ mice.

A-**E**. Under light:dark conditions, *Reverbα*$^{-/-}$ mice maintain robust diurnal rhythms in physiology and behaviour. Day/night food intake (**A**) (n=12-14/group), and energy expenditure (**B**) (n=3-4/group). Diurnal activity profile, mean activity (**C**) and body temperature (**D**) of adult male *Reverbα*$^{-/-}$ mice (activity is reported as the % daily activity, n=9-13/group). Diurnal profiles in oxygen consumption (VO_2) and carbon dioxide production (VCO_2) (**E**) (n=9-13/group). **F**. Western blot showing REVERBα expression in adipose tissue over 24 hours. **G**. Molar percentages of fatty acid species in WT and *Reverbα*$^{-/-}$ gWAT. n=6/group. [a]P<0.05. **H**. Daytime (ZT6) fasted blood glucose levels (n=11/group). **I**. *Reverbα*$^{-/-}$ mice are highly susceptible to diet-induced obesity, showing significantly higher body weights and fat mass than control mice after 10 weeks of HFD feeding (n=6/group). **J**. In a separate study, food intake was tracked for individual mice over 3 weeks of HFD feeding (n = 13/group). Mean daily food intake in *Reverbα*$^{-/-}$ mice showed a significant positive correlation with body weight.

Data presented as individual data points with mean (**A-D, H, I**), as mean +/- SEM (**F**), or as individual data points with line of best fit (**J**)**.** **P<0.01, two-way ANOVA with Tukey's multiple comparisons tests (**A**-**D**), unpaired t-tests with correction for multiple testing (**G**), unpaired two-tailed t-tests (**H**,**I**), linear regression (**J**).

storage of fatty acids and triglyceride in the knockout mice. To validate this putative increase in local lipid synthesis, we quantified fatty acid species in gWAT, and indeed, the ratio of palmitic to linoleic acid (C16:0/C18:2n6), a marker of *de novo* lipogenesis, was significantly elevated in *Reverbα*$^{-/-}$ samples (**Figure 1E, Figure 1 Supplemental G**). Fatty acid profiling also revealed evidence of increased SCD1 activity (C16:1n-7/C16:0). Enhanced fatty acid synthesis in gWAT of mice lacking REVERBα may be in part driven by increased glucose availability and adipose tissue uptake as previously suggested (Delezie et al., 2012), although we do not observe elevated blood glucose levels in the *Reverbα*$^{-/-}$ animals (**Figure 1 Supplemental H**). The propensity to lipid storage is further highlighted by the substantial obesity, compared to littermate controls, displayed by *Reverbα*$^{-/-}$ mice when challenged with 10 weeks of high-fat diet (HFD) (**Figure 1 Supplemental I**; Delezie et al., 2012; Hand et al., 2015). Interestingly, we observed a strong positive correlation between body weight and daily intake of HFD in the *Reverbα*$^{-/-}$ mice (**Figure 1 Supplemental J**), suggesting that HFD-induced hyperphagia exacerbates weight gain and obesity in the *Reverbα*$^{-/-}$ mice.

Limited impact of adipocyte-selective *Reverbα* deletion under basal conditions

To define the role of REVERBα specifically within WAT, we generated a new mouse line with loxP sites flanking *Reverbα* exons 2-6 (*Reverbα*$^{Flox2\text{-}6}$), competent for Cre-mediated conditional deletion (**Figure 2A**; Hunter et al., 2020). We crossed this mouse with the well-established adiponectin Cre-driver line (*Adipo*^{Cre}; Eguchi et al., 2011; Jeffery et al., 2014) to delete *Reverbα* selectively in adipocytes. This new line results in loss of *Reverbα* mRNA (**Figure 2B**) and protein (**Figure 2C**) expression in adipose tissue depots, as well as coordinate de-repression of *Bmal1,* upon Cre-mediated recombination.

In marked contrast to global *Reverbα*$^{-/-}$ mice, adult *Reverbα*$^{Flox2\text{-}6}$*Adipo*^{Cre} mice did not show an increase in adiposity when maintained on a standard chow diet (**Figure 2D**; n=7/group), with no differences in mean body weight, fat and lean mass observed. In parallel with this, we saw

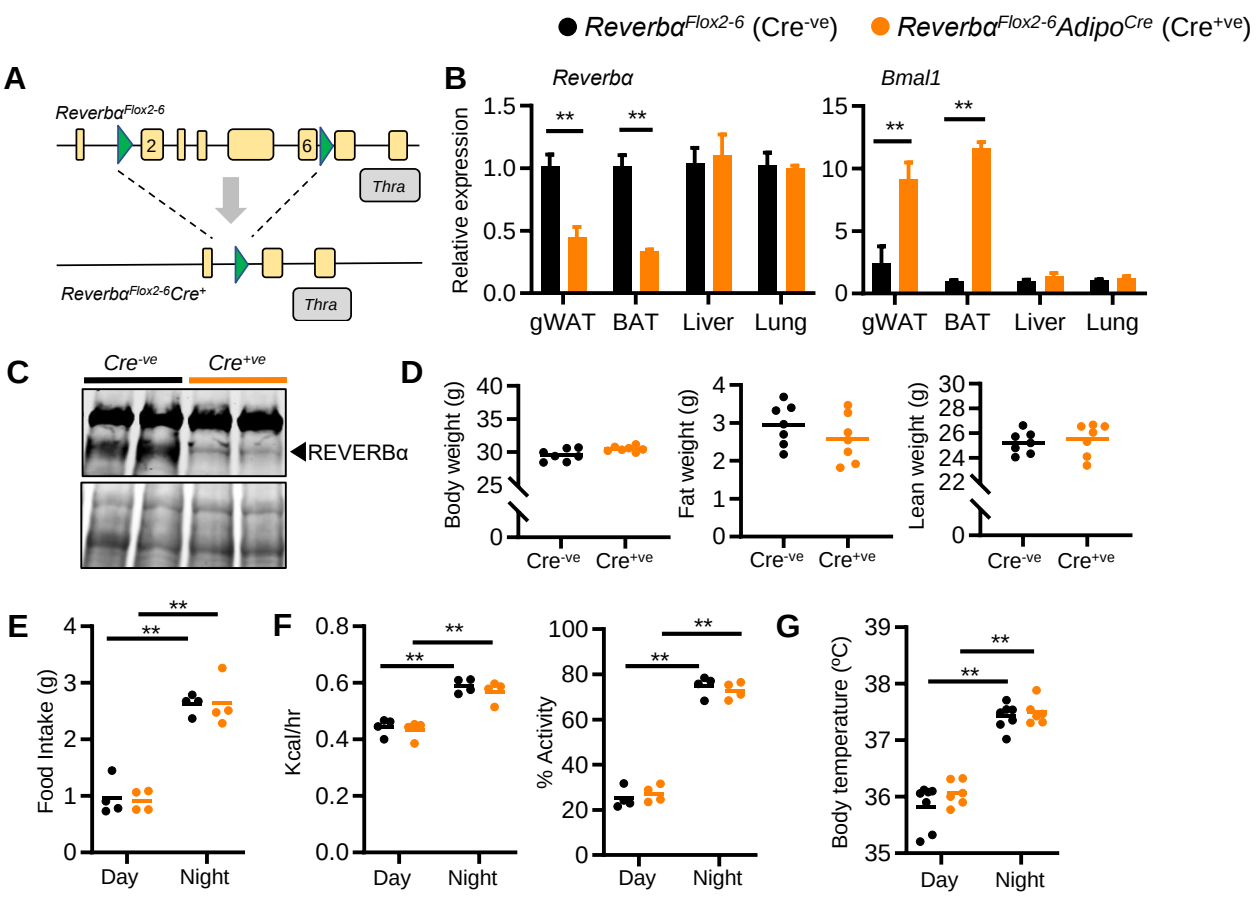

FIGURE 2. Impact of adipose *Reverbα* deletion is limited under normal conditions.
A. Targeting strategy for LoxP site integration flanking exons 2-6 of the *Nr1d1* (*Reverbα*) locus. **B**. *Reverbα* and *Bmal1* gene expression in gWAT, brown adipose (BAT), liver and lung in *Reverbα*$^{Flox2-6}$ (Cre^{-ve}) and *Reverbα*$^{Flox2-6}$*Adipo*^{Cre} (Cre^{+ve}) mice (n=4-5/group). **C**. REVERBα protein expression (arrowhead) in Cre^{-ve} and targeted Cre^{+ve} mice. Lower blot shows Ponceau S protein staining. **D**. Body weight, fat mass and lean mass in 13-week old Cre^{-ve} and Cre^{+ve} male mice (n=7/group). **E**-**G**. Both *Reverbα*$^{Flox2-6}$*Adipo*^{Cre} Cre^{+ve} and Cre^{-ve} mice demonstrate diurnal rhythms in behaviour and physiology, with no genotype differences observed in food intake (**E**), energy expenditure and daily activity (**F**) or body temperature (**G**) in 13-week old males (n=4-7/group).

Data presented as mean +/- SEM (**B**,) or as mean with individual data points (**D**-**G**). *P<0.05, **P<0.01, unpaired t-tests corrected for multiple comparisons (**B**), unpaired t-tests (**D**), two-way ANOVA with Tukey's multiple comparisons tests (**E**-**G**).

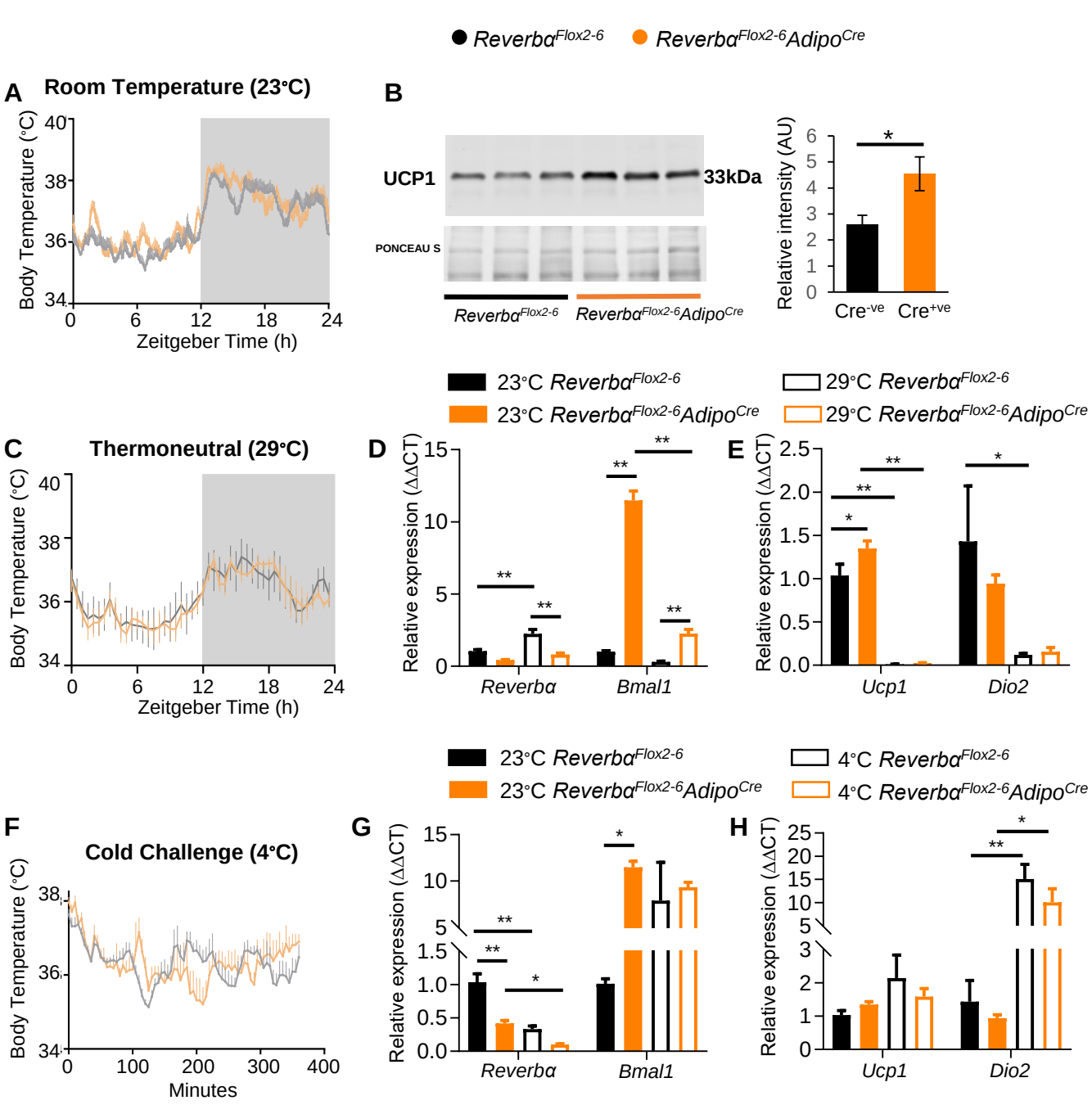

FIGURE 2 SUPPLEMENTAL. Loss of *Reverba* expression in brown adipocytes does not alter body temperature.

A-B. Housing under standard laboratory conditions did not alter daily profiles in body temperature in the *Reverbα*$^{Flox2\text{-}6}$*Adipo*^{Cre} Cre^{+ve} mice, when compared to control Cre^{-ve} littermate controls (**A**; n=5-6/group), despite showing increased UCP1 expression (**B**; n=3/group). **C**. No intergenotype genotype differences were observed in body temperature profiles recorded from mice housed under thermoneutral conditions (28-30°C) for 3 weeks (n=5-6/group). **D-E**. Brown adipose tissue (BAT) gene expression studies (qPCR) demonstrated expected de-repression of *Bmal1* expression in Cre^{+ve} mice, and expected reduction in *Ucp1* expression at thermoneutral conditions in both genotypes (compared to room temperature) (n=5-6/group). **F**. *Reverbα*$^{Flox2\text{-}6}$*Adipo*^{Cre} Cre^{+ve} mice and control littermates were exposed to an acute cold challenge (4°C for 6 h) with body temperature recording throughout (n=5-6/group). No genotype difference in thermogenic response was observed. **G-H.** As previously reported, *Reverbα* expression was reduced by cold exposure; however, no genotype differences were observed cold-induced increases in *Ucp1* or *Dio2* gene expression (n=5-6/group).

Data presented as mean +/- SEM. *P<0.05, **P<0.01, Student's t-test (**B**), 2-way ANOVA with Tukey's multiple comparisons tests (**D**, **E**, **G**, **H**).

no differences in daily patterns of food intake, energy expenditure, activity levels or body temperature in matched *Reverbα*$^{Flox2\text{-}6}$*Adipo*^{Cre} and control (*Reverbα*$^{Flox2\text{-}6}$) mice (**Figure 2D**,**E**).

As brown adipose tissue (BAT) makes an important contribution to whole body energy metabolism, we studied the thermoregulation of *Reverbα*$^{Flox2\text{-}6}$*Adipo*^{Cre} mice in greater detail. It has previously been proposed that REVERBα is key in conferring circadian control over thermogenesis, through its repression of uncoupling protein 1 (UCP1) (Gerhart-Hines et al., 2013). However, we saw no genotype differences in thermoregulation between *Reverbα*$^{Flox2\text{-}6}$*Adipo*^{Cre} and *Reverbα*$^{Flox2\text{-}6}$ mice (**Figure 2 Supplemental A-E**). Despite increased BAT UCP1 expression, no differences in body temperature profiles were observed between Cre^{-ve} and Cre^{+ve} mice when housed under normal laboratory temperature (~22ºC) nor when placed under thermoneutral conditions (29ºC) for >14days. Moreover, Cre^{-ve} and Cre^{+ve} mice did not differ in their thermogenic response to an acute cold challenge (4ºC for 6hr) (**Figure 2 Supplemental F-H**). Therefore, the minimal impact on body composition of adipose-targeted *Reverbα* deletion cannot be explained by altered BAT thermogenic activity, and moreover, these data challenge existing theories about the role of *Reverbα* in thermoregulation.

In normal WAT, REVERBα-regulated targets are limited to clock and collagen genes

To investigate adipocyte-specific *Reverbα* activity, we performed RNA-seq at ZT8 (n=6/group) in both *Reverbα*$^{-/-}$ and *Reverbα*$^{Flox2\text{-}6}$*Adipo*^{Cre} mouse lines. Global *Reverbα* deletion had a large effect on the gWAT transcriptome, with 4163 genes showing significant differential expression (FDR<0.05) between *Reverbα*$^{-/-}$ mice and age- and weight-matched WT littermate controls (**Figure 3A**). Pathway enrichment analysis demonstrated that these changes are dominated by metabolic genes (**Figure 3B(i)**), with lipid metabolism and the TCA cycle emerging as prominent processes (**Figure 3B(ii)**). Thus, the gWAT transcriptome in *Reverbα*$^{-/-}$ mice is concordant with the phenotype, and the gWAT proteome, in demonstrating up-regulation of lipid accumulation and storage processes.

By contrast, and consistent with the absence of an overt phenotype, only a small genotype effect on the transcriptome was observed when comparing gWAT RNA-seq from *Reverbα*$^{Flox2\text{-}6}$*Adipo*^{Cre} and *Reverbα*$^{Flox2\text{-}6}$ littermates (**Figure 3C**; n=6/group). Here, 238 genes showed significant differential expression between genotypes, of which 128 were also differentially regulated in the WAT analysis of global *Reverbα*$^{-/-}$ mice (**Figure 3D**). These 128 common genes included circadian clock components (*Bmal1, Clock, Cry2, Nfil3*), whilst pathway analysis also revealed collagen formation/biosynthesis processes to be significantly enriched (**Figure 3C**). Regulation of the molecular clock is expected, but the discovery of collagen dynamics as a target of REVERBα regulatory action in adipocytes has not been previously recognised. We validated consistent up-regulation of collagen and collagen-modifying genes in *Reverbα*$^{-/-}$ and *Reverbα*$^{Flox2\text{-}6}$*Adipo*^{Cre} gWAT by qPCR (**Figure 3F**).

It is notable that *Reverbα*$^{Flox2\text{-}6}$*Adipo*^{Cre} mouse gWAT exhibits neither enrichment of lipid metabolic pathways, nor de-regulation of individual key lipogenic genes, previously identified as REVERBα targets (**Figure 3E,G**) (Feng et al., 2011; Zhang et al., 2016, 2015). These findings suggest lipogenic gene regulation may be a response to system-wide changes in energy metabolism in the *Reverbα*$^{-/-}$ animals, and challenge current understanding of REVERBα action.

Work in liver has suggested that the REVERBα paralogue, REVERBβ, contributes to the suppression of lipogenesis, and that concurrent REVERBβ deletion amplifies the impact of REVERBα loss (Bugge et al., 2012). We therefore performed double knock-down of *Reverbα* and *Reverbβ* in differentiated 3T3-L1 cells (**Figure 3 Supplemental A**). Whilst double knock-down produced greater *Bmal1* de-repression than either *Reverbα* or *Reverbβ* knock-down alone, it did not lead to de-repression of lipogenic genes previously considered REVERBα targets (**Figure 3 Supplemental B**). This suggests that compensation by *Reverbβ* does not underlie the mild phenotype observed in the *Reverbα*$^{Flox2\text{-}6}$*Adipo*^{Cre} mice.

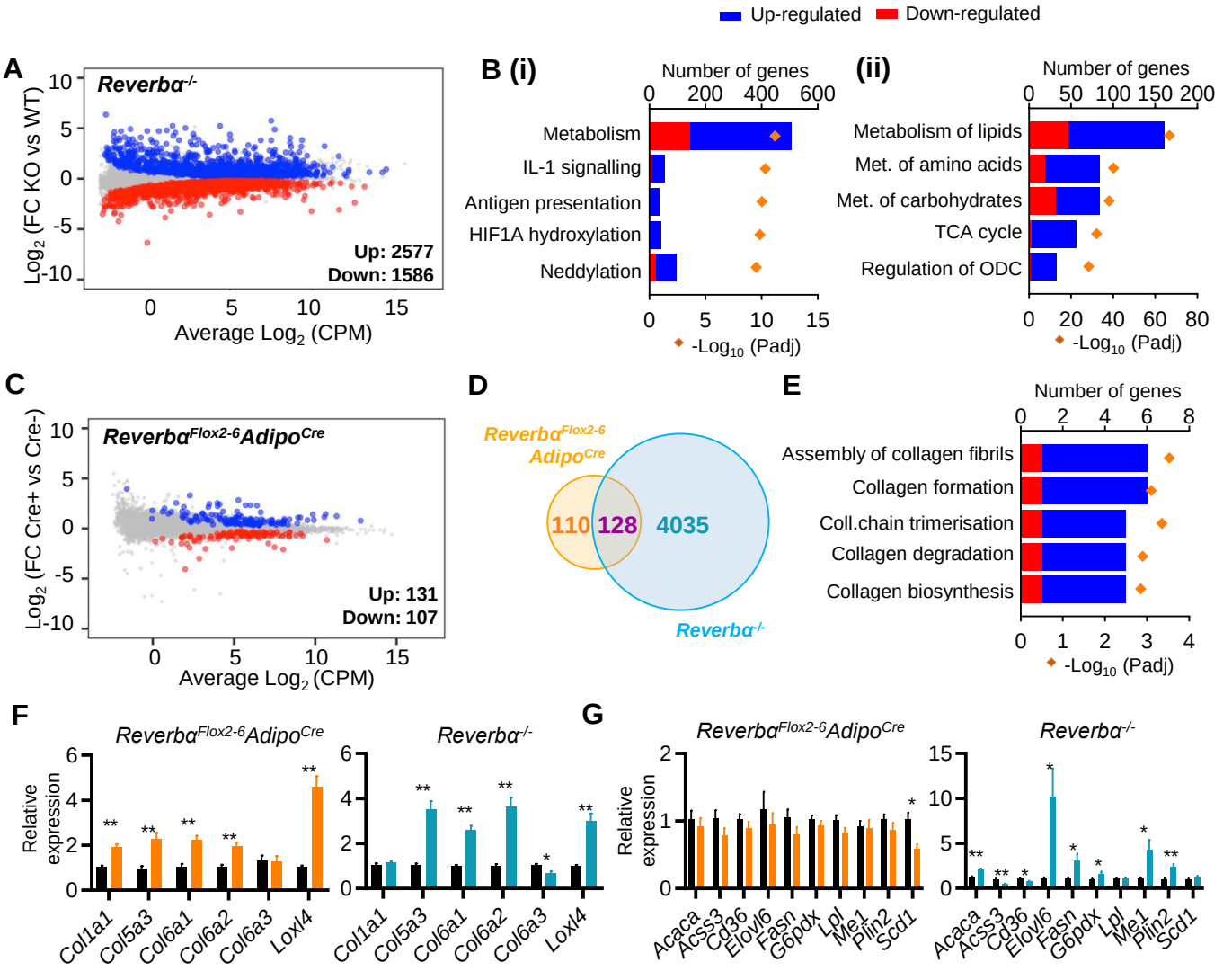

FIGURE 3. Global or adipose-specific *Reverbα* deletion produces distinctive gene expression profiles. **A, B**. *Reverbα*$^{-/-}$ gWAT demonstrates extensive remodelling of the transcriptome and up-regulation of metabolic pathways. Mean-difference (MD) plot (**A**) showing significantly (FDR<0.05) up- (blue) and down- (red) regulated genes in gWAT of *Reverbα*$^{-/-}$ mice compared to littermate controls (n=6/group). Pathway analysis (**B**) of significantly differentially expressed genes (FDR<0.05): top five (by gene count) significantly enriched Reactome terms shown (**B(i)**), top 5 metabolic pathways shown (**B(ii)**). Up-regulated genes in blue, down-regulated in red. ODC = ornithine decarboxylase. **C**. By contrast, RNA-seq demonstrates modest remodelling of the transcriptome in gWAT of *Reverbα*$^{Flox2\text{-}6}$*Adipo*^{Cre} mice. MD plot, n=6/group. **D**. Venn diagram showing overlap of differentially-expressed (DE) genes in *Reverbα*$^{Flox2\text{-}6}$*Adipo*^{Cre} and *Reverbα*$^{-/-}$ gWAT. **E**. Pathway analysis of 128 commonly DE genes. Top five (by gene count) significantly enriched Reactome terms shown. **F**,**G**. Collagen genes are commonly up-regulated in both genotypes (**F**), whilst genes of lipid metabolism are not DE in *Reverbα*$^{Flox2\text{-}6}$*Adipo*^{Cre} (**G**). gWAT qPCR, n=6-7/group.

Data presented as mean +/- SEM (**F, G**). *P<0.05, **P<0.01, unpaired t-tests corrected for multiple comparisons (**F, G**).

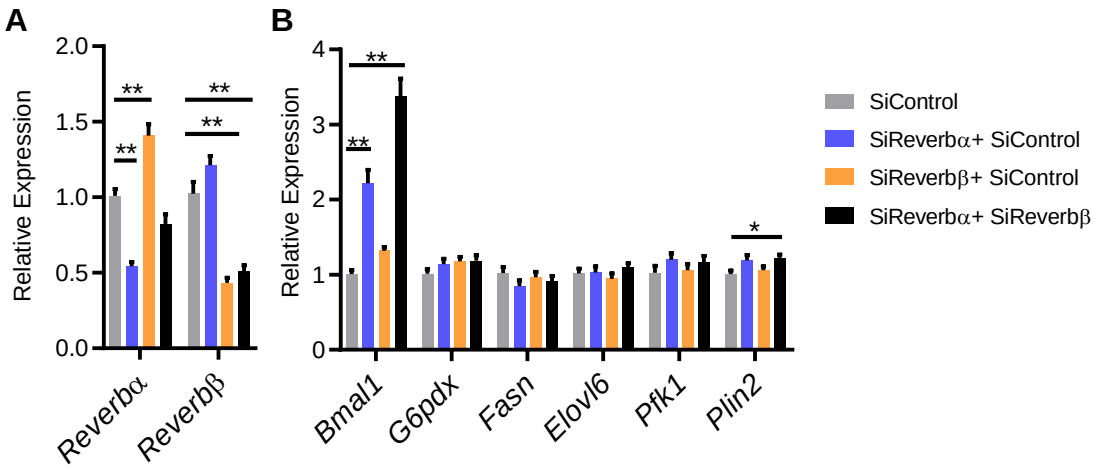

FIGURE 3 SUPPLEMENTAL. Impact of *Reverbα* and *Reverbβ* loss *in vitro.*
A, B. Double knockdown of *Reverbα* and *Reverbβ* in differentiated 3T3-L1 cells (**A**) results in marked de-repression of *Bmal1* expression but minimal effects on expression of typically pro-lipogenic genes (**B**) (data compiled from three replicated knockdown experiments, n=8-9/treatment group).

Data presented as mean +/- SEM. *P<0.05, **P<0.01, one-way ANOVA with Dunnett's multiple comparisons tests (**A**, **B**).

Thus, whilst global REVERBα targeting produces an adiposity phenotype with up-regulation of WAT lipogenesis and lipid storage, this is not seen when REVERBα is selectively targeted in adipose alone. The distinction is not due to loss of *Reverbα* expression in brown adipose, and is not due to compensatory REVERBβ action. Taken together, our data suggest that under a basal metabolic state, the adipose transcriptional targets under direct REVERBα control are in fact limited to core clock function and collagen dynamics. REVERBα is not a major repressor of lipid metabolism in this setting. This also suggests that the enhanced lipid accumulation phenotype of *Reverbα*$^{-/-}$ adipose tissue is either independent from adipose REVERBα entirely, or that the action of REVERBα in adipose is context-dependent.

Diet-induced obesity reveals a broader WAT phenotype in tissue-specific REVERBα deletion

Studies in liver tissue have demonstrated reprogramming of both nuclear receptor and circadian clock factor activity by metabolic challenge (Eckel-Mahan et al., 2013; Goldstein et al., 2017; Guan et al., 2018; Quagliarini et al., 2019). Both our data here, and previous reports (Delezie et al., 2012; Feng et al., 2011; Hand et al., 2015; Le Martelot et al., 2009; Preitner et al., 2002), highlight that the normal chow-fed *Reverbα*$^{-/-}$ mouse is metabolically abnormal. The emergence of the collagen dynamics as a direct REVERBα target and exaggerated diet-induced obesity evident in *Reverbα*$^{-/-}$ mice supports a role for REVERBα in regulating adipose tissue expansion under obesogenic conditions. To test this, *Reverbα*$^{Flox2\text{-}6}$*Adipo*^{Cre} and *Reverbα*$^{Flox2\text{-}6}$ mice were provided with HFD for 16 weeks to drive obesity and WAT expansion. Indeed, compared to their controls, *Reverbα*$^{Flox2\text{-}6}$*Adipo*^{Cre} mice exhibited greater weight gain and adiposity in response to HFD feeding (**Figure 4A,B**). Of note, divergence between control and *Reverbα*$^{Flox2\text{-}6}$*Adipo*^{Cre} mice became clear only after long-term HFD-feeding (beyond ~13 weeks), a time at which body weight gain plateaus in control mice. This contrasts substantially with *Reverbα*$^{-/-}$ mice, which show rapid and profound weight gain from the start of HFD feeding (Hand et al., 2015). The stark difference in progression and severity of diet-induced obesity is likely due (at least in part) to the HFD-induced hyperphagia, which is observed in *Reverbα*$^{-/-}$

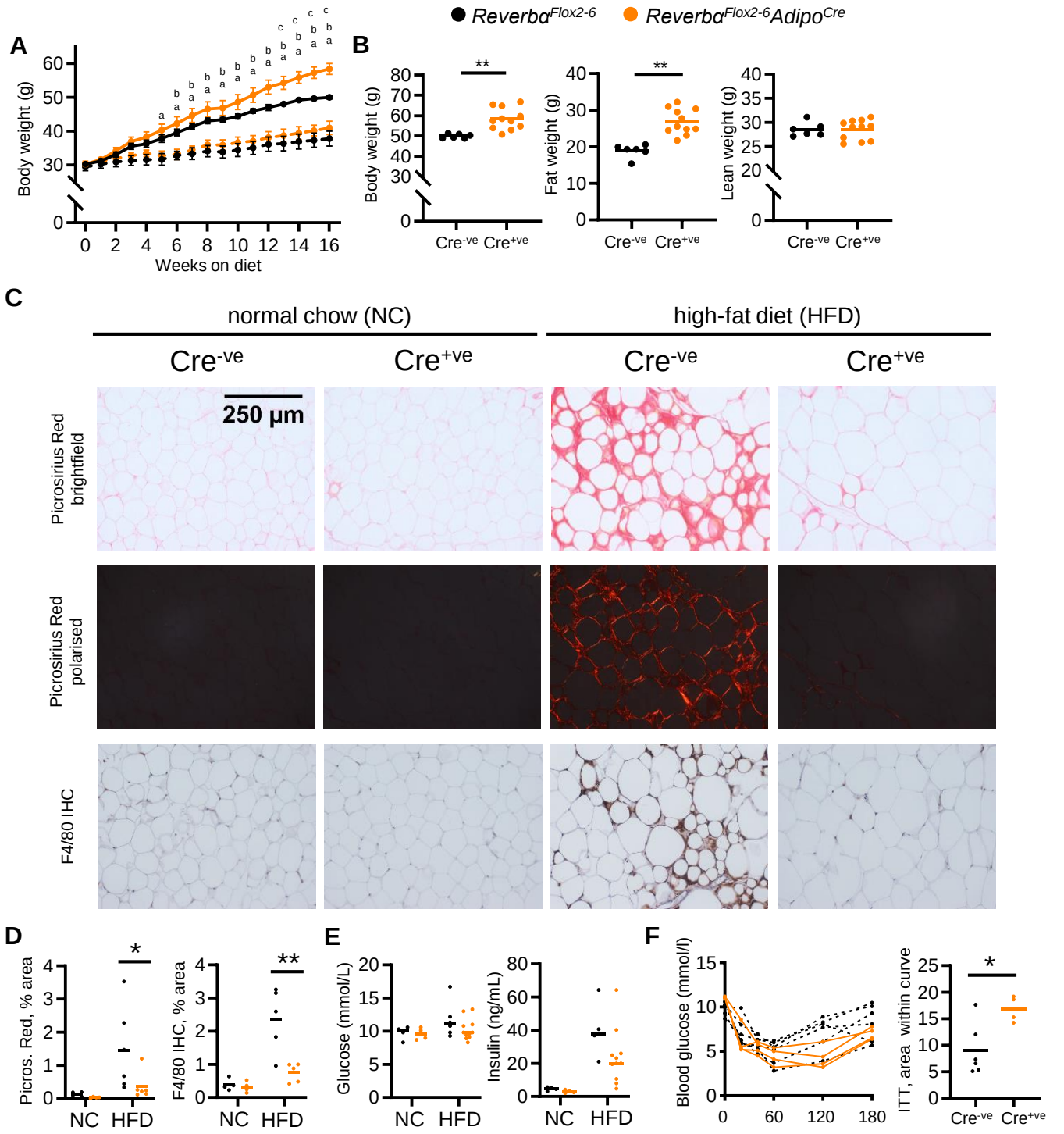

FIGURE 4. Diet-induced obesity unmasks a role for REVERBα in the regulation of adipose expansion. **A**, **B**. High-fat diet leads to exaggerated adiposity in *Reverbα*$^{Flox2\text{-}6}$*Adipo*^{Cre} mice. Body weight track of Cre^{-ve} and Cre^{+ve} male mice on high-fat diet (solid line) or normal chow (dashed line) (**A**) (^{a}P<0.05: Cre^{+ve} NC vs HFD; ^{b}P<0.05, Cre^{-ve} NC vs HFD; ^{c}P<0.05, Cre^{+ve} HFD vs Cre^{-ve} HFD); total body, fat and lean weight after 16 weeks in the high-fat diet group (**B**). **C**,**D**. On histological examination of WAT, HFD-fed Cre^{+ve} mice display less fibrosis and inflammation than Cre^{-ve} littermates. Representative Picrosirius Red and F4/80 immunohistochemistry images (x20 magnification) (**C**), quantification of staining across groups, each data point represents the mean value for each individual animal (**D**). **E**,**F**. Despite increased adiposity, HFD-fed Cre^{+ve} mice display greater insulin sensitivity than Cre^{-ve} controls. Terminal blood glucose and insulin levels (animals culled 2hrs after food withdrawal) in NC and HFD-fed in *Reverbα*$^{Flox2\text{-}6}$*Adipo*^{Cre} Cre^{-ve} (black) and Cre^{-ve} (orange) mice (**E**). Blood glucose values for individual animals and area within curve for 16-week HFD-fed *Reverbα*$^{Flox2\text{-}6}$*Adipo*^{Cre} Cre^{-ve} and Cre^{-ve} mice undergoing insulin tolerance testing (ITT) (**F**).

Data presented as mean +/- SEM (**A**) or as individual data points with mean (**B**, **D**, **E**, **F**). *P<0.05, **P<0.01, two-way repeated measures ANOVA with Tukey's multiple comparisons tests (**A**), two-way ANOVA with Sidak's multiple comparisons tests (**D**, **E**), unpaired two-tailed t-test (**B**, **F**). n=4-11/group for all panels.

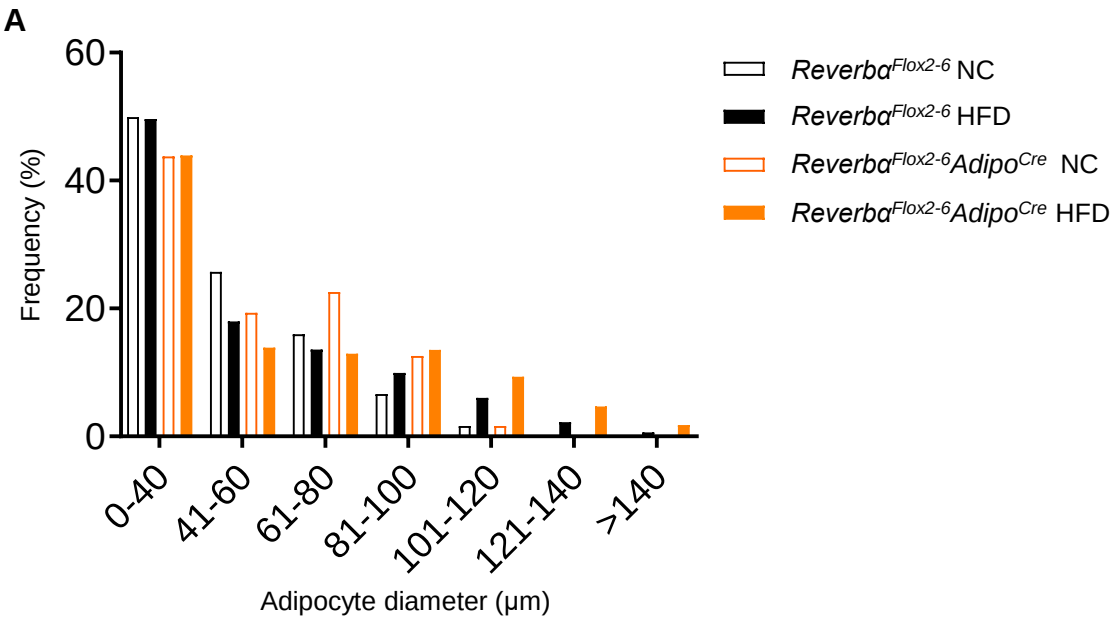

FIGURE 4 SUPPLEMENTAL. Adipocyte size in *Reverbα*$^{Flox2-6}$ and *Reverbα*$^{Flox2-6}$*Adipo*^{Cre} mice .
A. Quantification of WAT adipocyte size in NC- and HFD-fed *Reverbα*$^{Flox2-6}$ and *Reverbα*$^{Flox2-6}$*Adipo*^{Cre} mice demonstrates no between-genotype differences in size distribution. n=4-6/group.

Data presented as mean. Two-way ANOVA with Tukey's multiple comparisons tests.

mice (WT food intake 2.92 ±0.10g HFD/day/mouse; KO 3.74 ±0.21g, P=0.0014, Student's T-test, n=21/genotype), but not in *Reverbα*$^{Flox2\text{-}6}$*Adipo*^{Cre} mice (Cre^{-ve} 2.99 ±0.61g HFD/day/mouse; Cre^{+ve} 3.01 ±0.60g, P>0.05, n=8/genotype). Nevertheless, both models highlight that loss of REVERBa increases capacity for increased lipid storage and adipose tissue expansion under obesogenic conditions.

Despite the enhanced diet-induced obesity, HFD-fed *Reverbα*$^{Flox2\text{-}6}$*Adipo*^{Cre} mice showed little evidence of typical obesity-related pathology. Histological assessment of gWAT after 16-weeks of HFD feeding revealed widespread adipose tissue fibrosis (Picrosirius Red staining of collagen deposition under normal and polarised light) and macrophage infiltration (F4/80 immunohistochemistry) in obese control mice, but these features were not seen in *Reverbα*$^{Flox2\text{-}6}$*Adipo*^{Cre} mice (**Figure 4C,D**). Furthermore, we saw evidence of preserved insulin sensitivity in the HFD-fed *Reverbα*$^{Flox2\text{-}6}$*Adipo*^{Cre} mice, with neither circulating glucose nor insulin being higher than *Reverbα*$^{Flox2\text{-}6}$ littermate controls (**Figure 4E**), despite carrying significantly greater fat mass. Indeed, on insulin tolerance testing, HFD-fed *Reverbα*$^{Flox2\text{-}6}$*Adipo*^{Cre} mice demonstrated more marked hypoglycaemia than HFD-fed controls (**Figure 4F**). We saw no differences in adipocyte size between the two genotypes, indicating that our observations did not simply reflect greater adipocyte hyperplasia in the *Reverbα*$^{Flox2\text{-}6}$*Adipo*^{Cre} mice (**Figure 4 Supplemental A**).

Therefore, under long-term HFD-feeding conditions, adipose-targeted *Reverbα* deletion results in continued adipose tissue expansion accompanied by a healthier metabolic phenotype with reduced adipose inflammation and fibrosis, and preserved systemic insulin sensitivity. Importantly, these findings also suggest that the regulatory influence of REVERBα is context-dependent, with the metabolic impact of adipose-targeted *Reverbα* deletion revealed by transition to an obese state.

REVERBα-dependent gene regulation is reprogrammed by obesity

We next performed RNA-seq on gWAT collected at ZT8 from *Reverbα*$^{Flox2\text{-}6}$*Adipo*^{Cre} and *Reverbα*$^{Flox2\text{-}6}$ littermate controls fed either normal chow (NC) or HFD for 16 weeks (NC, n=4/group; HFD, n=6/group). As expected, HFD-feeding had a substantial impact on the gWAT transcriptome in both Cre^{-ve} and Cre^{+ve} animals (i.e. NC vs HFD comparison within each genotype; **Figure 5A**). Under NC feeding conditions, we again observed only a small genotype effect on the transcriptome, and as before, differentially-expressed genes included core clock genes (*Bmal1, Nfil3, Npas2, Clock*) and those of collagen synthesis pathways (**Figure 5B**). However, obesity revealed a substantial genotype effect, with 3061 genes differentially expressed (1706 up, 1355 down) in HFD-fed *Reverbα*$^{Flox2\text{-}6}$*Adipo*^{Cre} mice versus HFD-fed *Reverbα*$^{Flox2\text{-}6}$ controls (**Figure 5B**), and 1704 genes showing a significant ($\alpha<0.05$) diet-genotype interaction (stageR specific interaction analysis; Van den Berge et al., 2017). Of these 1704 genes, those up-regulated in obese *Reverbα*-deficient adipose were strongly enriched for metabolic pathways, whilst down-regulated genes showed weak enrichment of ECM organisation processes (**Figure 5C**). To examine how loss of *Reverbα* alters adipose tissue response to diet-induced obesity, we compared directly those processes which showed significant obesity-related dysregulation in control mice (**Figure 5D**). While HFD-feeding caused a profound down-regulation (vs NC conditions) of metabolic pathways in the WAT of control mice, this was not observed in *Reverbα*$^{Flox2\text{-}6}$*Adipo*^{Cre} mice. By contrast, HFD-feeding led to an up-regulation of immune pathways in both genotypes (**Figure 5D**). Thus, transcriptomic profiling correlates with phenotype in suggesting that WAT function and metabolic activity is protected from obesity-related dysfunction in the *Reverbα*$^{Flox2\text{-}6}$*Adipo*^{Cre} mice, and that the impact of adipose *Reverbα* deletion is dependent on system-wide metabolic state.

Integration of differential gene expression with the WAT cistrome reveals state-dependent regulation of metabolic targets by REVERBα

To examine the mechanism of REVERBα regulation of the WAT metabolic programme in HFD-fed mice, we analysed the relationship between differentially expressed genes revealed by

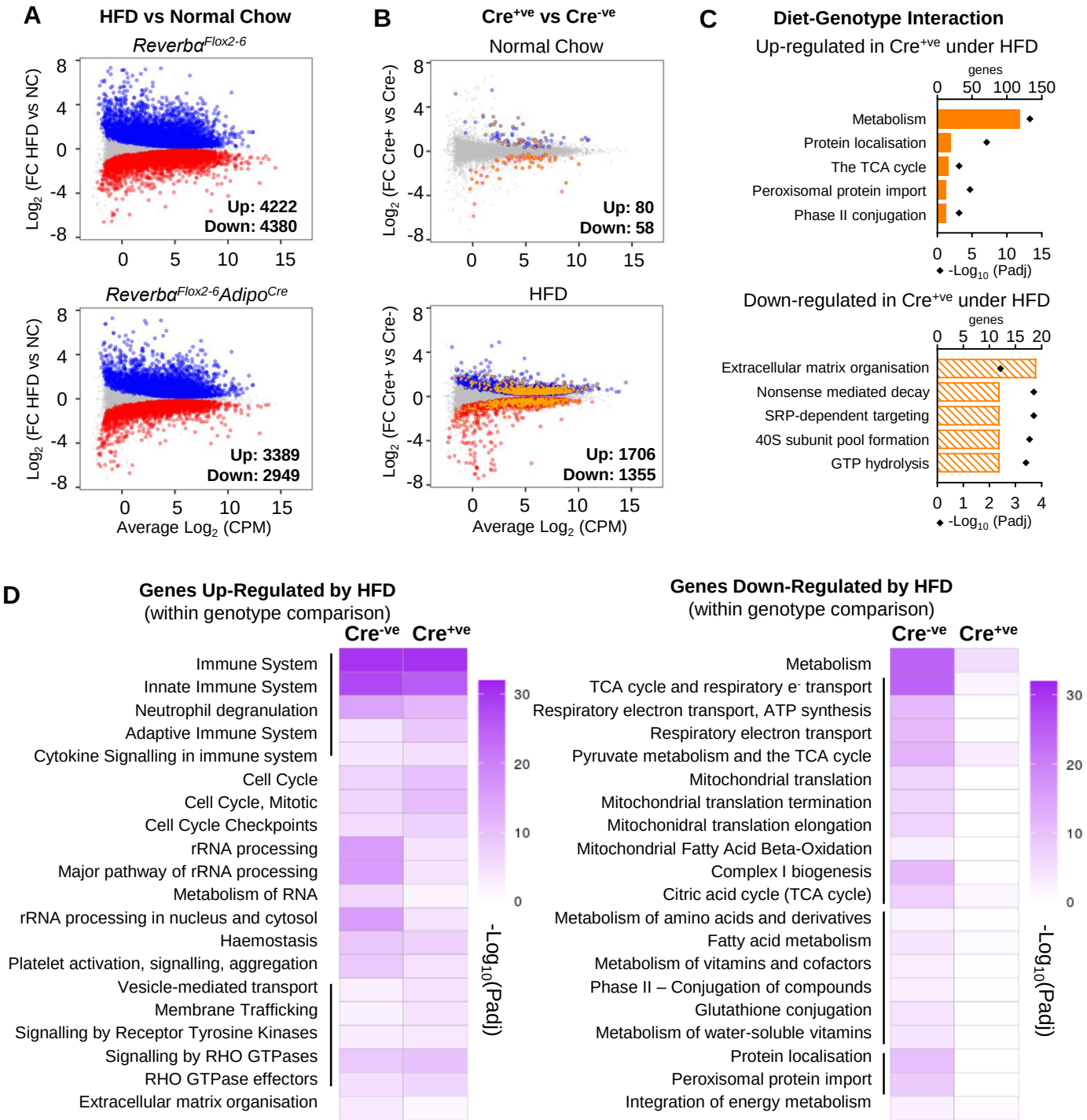

FIGURE 5. Under conditions of obesity, REVERBα repression extends to metabolic pathways.
A. High-fat diet dramatically remodels the WAT transcriptome. RNA-seq (n=4-6/group) was performed in gWAT from Cre^{-ve} and Cre^{+ve} male mice fed normal chow (NC) or high-fat diet (HFD) for 16 weeks. MD plots show genes significantly (FDR<0.05) up-regulated (blue) or down-regulated (red) by HFD in each genotype. **B**. With HFD, the REVERBα-responsive gWAT transcriptome broadens. MD plots show effect of genotype in NC (top panel) and HFD (lower panel) feeding conditions. Genes where stageR detects a significant (α=0.05) genotype-diet interaction highlighted in orange. **C**. Reactome pathway analysis of genes up- or down-regulated in Cre^{+ve} gWAT under HFD conditions, where this diet-genotype interaction is also detected. Top five (by gene count) significantly enriched terms shown. **D**. Adipose-targeted deletion of *Reverbα* attenuates the normal HFD-induced down-regulation of metabolic pathways. Heatmaps show enrichment (-log$_{10}$(Padj)) of Reactome pathways in genes up-regulated (left) or down-regulated (right) by HFD feeding in Cre^{-ve} and Cre^{+ve} gWAT. Top twenty (by gene count in Cre^{-ve} group) significantly enriched terms shown.

our RNA-seq studies and the WAT REVERBα cistrome. We identified primary REVERBα target genes by comparing genes changing in *Reverbα*$^{Flox2\text{-}6}$*Adipo*^{Cre} gWAT (relative to control mice, under both NC and HFD conditions) with genes changing in *Reverbα*$^{-/-}$ gWAT. To define the cistrome, we used raw published gWAT ChIP-seq data (Zhang et al., 2015) to call 2,354 high-stringency REVERBα peaks. To infer which genes might be direct targets of REVERBα repression, we employed a custom Python script that calculates the enrichment of differentially expressed gene sets in spatial relation to identified transcription factor binding sites (**Figure 6 Supplemental A**) (Hunter et al., 2020; Yang et al., 2019), over all genes in the genome.

Under NC conditions, only small sets of genes were up- or down-regulated in both *Reverbα*$^{Flox2\text{-}6}$*Adipo*^{Cre} and *Reverbα*$^{-/-}$ tissues (versus their respective controls) (**Figure 6A(i,ii)**). Nevertheless, genes up-regulated in *Reverbα*$^{Flox2\text{-}6}$*Adipo*^{Cre} and *Reverbα*$^{-/-}$ gWAT were significantly enriched around REVERBα ChIP-seq peaks at distances up to 1Mbp (**Figure 6A(i)**), consistent with repression mediated directly by DNA-bound REVERBα. Of these genes, 61.8% were within 100kbp of a stringent REVERBα peak, strongly suggesting that this gene cluster (clock and collagen genes) represents direct targets of REVERBα repression in WAT under NC conditions. Genes up-regulated only in *Reverbα*$^{-/-}$ WAT were also enriched around REVERBα peaks (at distances of up to 500kbp) suggesting that at least a proportion of these genes are presumptive direct targets of REVERBα regulation. In contrast, no enrichment of genes with decreased expression in *Reverbα*$^{Flox2\text{-}6}$*Adipo*^{Cre} or *Reverbα*$^{-/-}$ WAT was evident at any distance from REVERBα peaks (**Figure 6A(ii)**). Thus, REVERBα activation of transcription involves a different mechanism of regulation, likely involving secondary or indirect mechanisms (e.g. de-repression of another repressor), as previously proposed to explain REVERBα transactivation (Le Martelot et al., 2009).

HFD-feeding of *Reverbα*$^{Flox2\text{-}6}$*Adipo*^{Cre} mice greatly increased the overlap of differentially-expressed genes with those differentially expressed in *Reverbα*$^{-/-}$ WAT. (**Figure 6A(iii,iv)**). We observed a highly significant proximity enrichment of these commonly up-regulated genes

(863) to sites of REVERBα chromatin binding (**Figure 6A(iii)**), but again, saw no enrichment of the commonly down-regulated genes (**Figure 6A(iv)**). This integration of transcriptome and cistrome profiling suggests that REVERBα's exertion of direct repressive control over gene targets is dependent on metabolic state, and increases substantially under HFD-feeding conditions. Of note, the 1714 genes up-regulated only in the *Reverbα*$^{-/-}$ WAT retained some proximity enrichment to REVERBα binding sites. This suggests that some of these genes are direct REVERBα targets but subject to additional transcriptional controls.

Consistent with the healthier metabolic phenotype and transcriptome changes observed in obese *Reverbα*$^{Flox2\text{-}6}$*Adipo*^{Cre} mice, we found that the large majority of the 863 REVERBα gene targets unmasked by HFD-feeding are normally repressed in obesity (**Figure 6B**), with 551 (63.8%) being significantly down-regulated in obese control (Cre^{-ve}) animals. These genes include important regulators of lipid and mitochondrial metabolism (**Figure 6C**) - including *Fasn, Scd1, Dgat2, Cs* - and FGF-21 co-receptor *Klb*, a previously-identified REVERBα target gene (Jager et al., 2016). Considered together, these findings suggest that the healthy adiposity phenotype in HFD-fed *Reverbα*$^{Flox2\text{-}6}$*Adipo*^{Cre} mice results from de-repression of REVERBα-controlled pathways allowing continued and efficient lipid synthesis and storage, thus permitting greater expansion of the adipose bed and attenuation of obesity-related dysfunction.

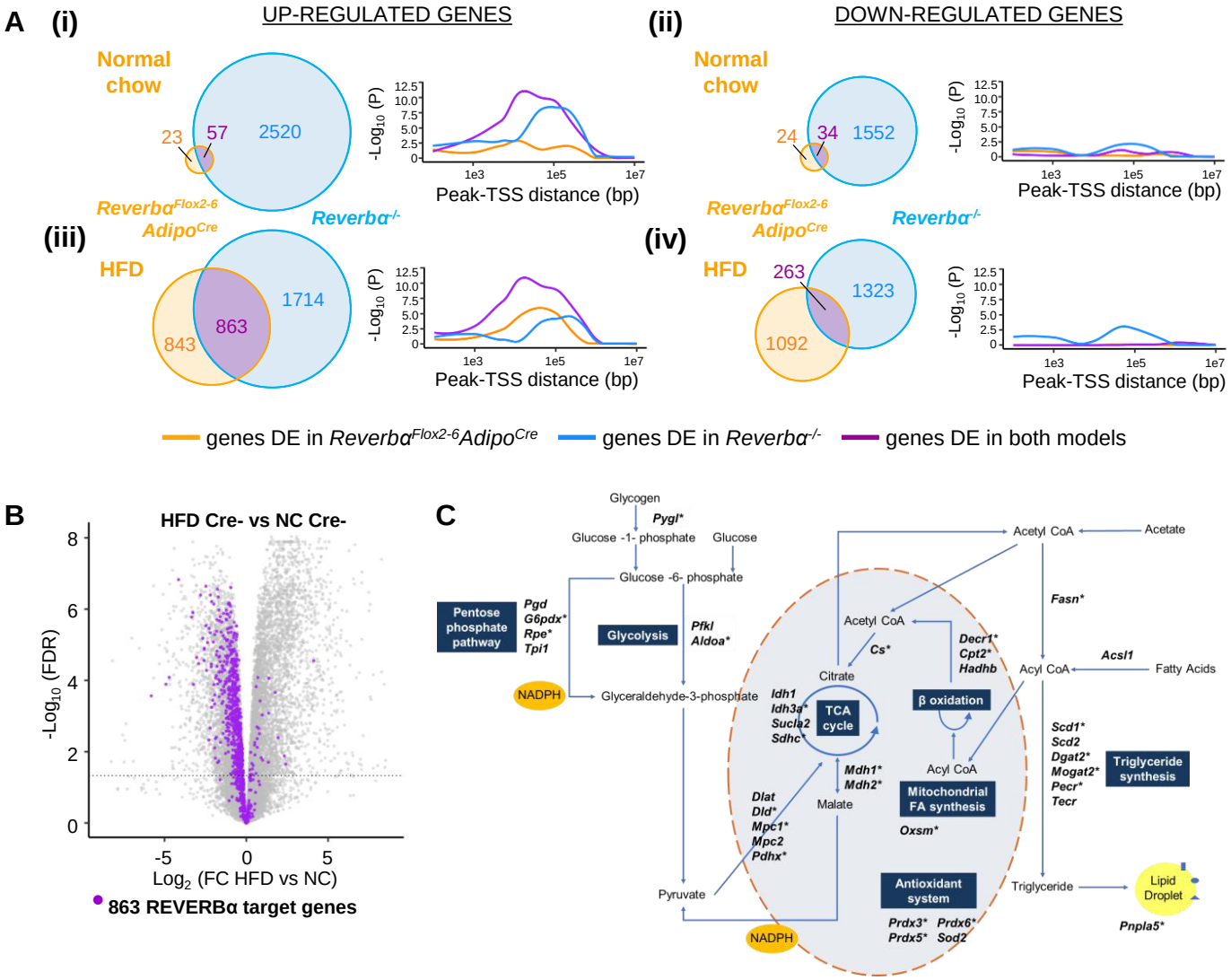

FIGURE 6. REVERBα-regulated targets, unmasked by obesity, associate with gWAT REVERBα binding sites.

A. Genes commonly up-regulated by *Reverbα* loss, in both the basal and obese state, show the strongest association with gWAT REVERBα ChIP-seq peaks. Venn diagrams show overlap of differentially-expressed (DE) genes in *Reverbα*$^{Flox2\text{-}6}$*Adipo*^{Cre} Cre^{+ve} mice (under NC (**i, ii**) and HFD (**iii**,**iv**) conditions) with differentially-expressed genes in *Reverbα*$^{-/-}$ mice (each compared to their respective controls). Plots show –log$_{10}$(P-value for enrichment) for each gene cluster at increasing distances from stringent REVERBα gWAT ChIP-seq peaks (FE>7.5 over input). See Figure 6 Supplemental (A) for schematic. DE genes separated by direction of regulation (up or down). **B**,**C**. REVERBα targets are also down-regulated in obesity, and include important lipid and mitochondrial metabolic regulators. Volcano plot (**B**) highlighting effect of HFD (in intact (Cre^{-ve}) animals) of the 863 REVERBα target genes from **A(iii)**. Metabolic map illustrating REVERBα targets (**C**). Genes showing significantly down-regulation by HFD (in Cre^{-ve} animals) are starred*.

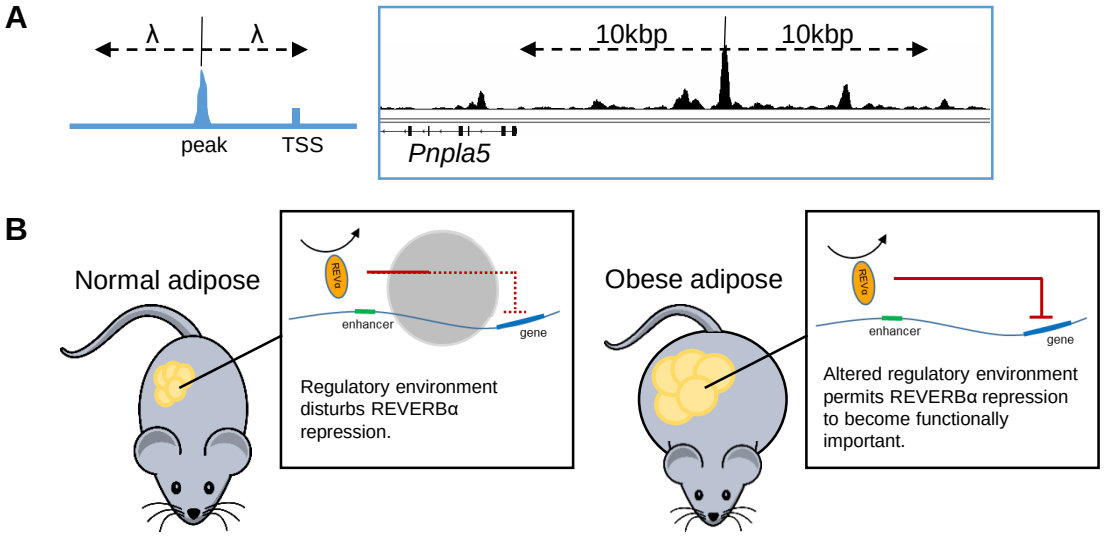

FIGURE 6 SUPPLEMENTAL. Relationship between REVERBα binding sites and gene regulation.
A. Schematic of peaks-genes analysis. ChIP-seq peaks are extended by user-specified distances (λ) either side of the peak centre. Enrichment of the genes of interest, within all genes whose transcription start site (TSS) is detected within λ, is assessed by a hypergeometric test. The TSS of *Pnpla5*, for example, lies within 10kbp of a REVERBα ChIP-seq peak. **B**. Proposed model. In normal conditions, there is a large number of genes over which REVERBα repressive control is not apparent, likely because the regulatory environment (chromatin state, presence of other regulators) blocks this interaction or renders it redundant. In obese adipose, alterations to the regulatory environment (e.g. chromatin remodelling) are permissive to REVERBα activity.

DISCUSSION

We set out to define the role of REVERBα in the regulation of white adipose tissue metabolism, and subsequently reveal a new understanding of REVERBα function. Together, our data show REVERBα to be a state-dependent regulator of WAT metabolism, with its widespread repressive action only unmasked by diet-induced obesity. Surprisingly, *Reverbα* expression in WAT appears to limits the energy buffering function of the tissue. This finding parallels our recent work in the liver (Hunter et al., 2020). Hepatic-selective loss of REVERBα carries no metabolic consequence, with REVERBα-dependent control over hepatic energy metabolism revealed only upon altered feeding conditions. Contrary to current understanding, our findings therefore suggest that REVERBα (and potentially other components of the peripheral clock) does not impose rhythmic repression of metabolic circuits under basal conditions, but rather determines tissue responses to altered metabolic state.

As reported previously by us and others (Delezie et al., 2012; Hand et al., 2015), global deletion of *Reverbα* leads to an increase in lipogenesis, adipose tissue expansion, and an exaggerated response to diet-induced obesity. How the loss of REVERBα specifically in WAT contributes to this phenotype has not previously been addressed. Here, we use proteomic, transcriptomic and lipid profiling studies to show a clear bias towards fatty acid synthesis and triglyceride storage within *Reverbα*$^{-/-}$ WAT. Adipocyte-targeted deletion of *Reverbα* reveals only a modest phenotype, and a relatively selective set of gene targets, limited to clock processes and collagen dynamics. These genes are concurrently de-regulated in *Reverbα*$^{-/-}$ adipose, and are found in proximity to REVERBα binding sites, strongly implicating them as direct targets of REVERBα repressive activity.

The reduced inflammation seen in obese *Reverbα*$^{Flox2\text{-}6}$*Adipo*^{Cre} mice is likely multifactorial, but may be secondary to a reduction in the pro-inflammatory free fatty acid pool, resulting from de-repression of lipogenic and mitochondrial metabolism pathways, or the absence of signals

366 from dead/dying adipocytes. It is of note that improved metabolic flexibility is proposed to be
367 beneficial in other mouse models of metabolic disease (Jonker et al., 2012; Kim et al., 2007;
368 Virtue et al., 2018) and in human obesity (Aucouturier et al., 2011; Begaye et al., 2020). We
369 identify extracellular matrix as a new direct target of adipose REVERBα action; altered
370 regulation of WAT collagen production and modification is also likely to contribute to the rapid
371 and continued adipose tissue expansion and reduced obesity-related fibrosis. The clock has
372 been linked to ECM re-modelling in other tissues (Chang et al., 2020; Dudek et al., 2015;
373 Sherratt et al., 2019), where it is thought to coordinate ECM dynamics, collagen turnover and
374 secretory processes (Chang et al., 2020). Adipose-specific deletion of *Reverbα* now provides
375 a unique model to explore the complex ECM responses which accompany obesity-related
376 tissue hypertrophy and development of fibrosis.
377
378 A role for the clock in the regulation of WAT function has been reported in the literature
379 (Barnea et al., 2015; Paschos et al., 2012; Shostak et al., 2013), perhaps implying that it is
380 the rhythmicity conferred by the clock which is important for WAT metabolism. However,
381 despite robust rhythms of clock genes persisting, rhythmic gene expression in gWAT is largely
382 attenuated following genetic disruption of SCN function (Kolbe et al., 2016). This supports the
383 alternative notion that an intact local clock is not the primary driver of rhythmic peripheral tissue
384 metabolism. Indeed, metabolic processes, including lipid biosynthesis, were highly enriched
385 in the cohort of SCN-dependent rhythmic genes from this study (Kolbe et al., 2016), implying
386 that feeding behaviour and WAT responses to energy flux are more important than locally-
387 generated rhythmicity for adipose function.
388
389 The modest impact of adipose-selective *Reverbα* deletion is both at odds with the large effect
390 of global *Reverbα* deletion, and with the extensive WAT cistrome identified for REVERBα
391 (even by stringent peak calling as we have done here). This suggests that the tissue-specific
392 actions of REVERBα are necessary, but not sufficient, and require additional regulation from
393 the metabolic state. Although not explored to the same extent, a lipogenic phenotype of liver-

specific RORα/γ deletion has previously been shown to be unmasked by HFD-feeding (Zhang et al., 2017). By driving adipose tissue hypertrophy through HFD-feeding of the *Reverbα*$^{Flox2\text{-}6}$*Adipo*^{Cre} mice, we observed a stark difference in the adipose phenotype of targeted mice and littermate controls. WAT tissue lacking *Reverbα* showed significantly increased tissue expansion, but little evidence of normal obesity-related pathology (tissue fibrosis, and immune cell infiltration/inflammation). Genes controlling mitochondrial activity, lipogenesis and lipid storage were relatively spared from the obesity-related down-regulation observed in control mouse tissue, and were associated with the WAT REVERBα cistrome. Thus, in response to HFD-feeding, REVERBα acts to repress metabolic activity in the adipocyte and limit tissue expansion (albeit at the eventual cost of tissue dysfunction, inflammation and development of adipose fibrosis).

The broadening of REVERBα's regulatory influence in response to obesity likely reflects a change to the chromatin environment in which REVERBα operates (**Figure 6 Supplementary B**). The majority of emergent REVERBα target genes are repressed in obese adipose when *Reverbα* expression is intact (**Figure 6B**). As these genes are not de-repressed by *Reverbα* loss in normal adipose, REVERBα activity must be redundant or ineffective in a 'basal' metabolic state. Subsequent emergence of REVERBα's transcriptional control may reflect alterations in chromatin accessibility or organisation, and/or the presence of transcriptional repressors and accessory factors required for full activity. As REVERBα is itself proposed to regulate enhancer-promoter loop formation (Kim et al., 2018), modulation of *Reverbα* expression would be a further important variable here. Such reshaping of the regulatory landscape likely occurs across tissues, and may explain why, with metabolic challenge, emergent circadian rhythmicity is observed in gene expression (Eckel-Mahan et al., 2013; Kinouchi et al., 2018; Tognini et al., 2017), and in circulating and tissue metabolites (Dyar et al., 2018; Eckel-Mahan et al., 2013).

Here, we now uncover a role for REVERBα in limiting the energy-buffering role of WAT, a discovery which may present therapeutic opportunity as we cope with an epidemic of human obesity. Despite recent findings which have cast doubt on the utility of some of the small molecule REVERBα ligands (Dierickx et al., 2019), antagonising WAT REVERBα now emerges as a potential target in metabolic disease. Finally, our study suggests that a functioning circadian clock may be beneficial in coping with acute mistimed metabolic cues but, that under chronic energy excess, may contribute to metabolic dysfunction and obesity-related pathology.

MATERIALS AND METHODS

Animal experiments. All experiments described here were conducted in accordance with local requirements and licenced under the UK Animals (Scientific Procedures) Act 1986, project licence number 70/8558 (DAB). Procedures were approved by the University of Manchester Animal Welfare and Ethical Review Body (AWERB). Unless otherwise specified, all animals had *ad libitum* access to standard laboratory chow and water, and were group-housed on 12hour:12hour light:dark (LD) cycles and ambient temperature of 22°C+/-1.5°C. Male mice (*Mus musculus*) were used for all experimental procedures. All proteomics studies were carried out on 13-week-old weight matched males. RNA-seq studies for Figure 3 were carried out on 12-14 week-old weight-matched males; the RNA-seq study for Figure 5 was carried out on 28 week-old males (following 16 weeks of high-fat diet or normal chow feeding).

***Reverbα*$^{-/-}$**

Reverbα$^{-/-}$ mice were originally generated by Ueli Schibler (University of Geneva) (Preitner et al., 2002). These mice were created by replacing exons 2-5 of the *Reverbα* gene by an in-frame LacZ allele. Mice were then imported to the University of Manchester and backcrossed to C57BL/6J mice.

***Reverbα*$^{Flox2\text{-}6}$**

A CRISPR-Cas9 approach was used to generate a conditional knock allele for *Nr1d1* (*Reverbα*), as described (Hunter et al., 2020). LoxP sites were integrated, in a two-step process, at intron 2 and intron 6, taking care to avoid any previously described transcriptional regulatory sites (Yamamoto et al., 2004). A founder animal with successful integration of both the 5' and 3' loxP sites, transmitting to the germline, was identified and bred forward to establish a colony.

***Reverbα*$^{Flox2\text{-}6}$*Adipo*^{Cre}**

458 *Adiponectin*-driven Cre-recombinase mice (Eguchi et al., 2011; Jeffery et al., 2014) were
459 purchased from The Jackson Laboratory and subsequently bred against the *Reverbα*$^{Flox2\text{-}6}$ at
460 the University of Manchester.
461
462 **In vivo phenotyping.** Body composition of mice was analysed prior to cull by quantitative
463 magnetic resonance (EchoMRI 900). Energy expenditure was measured via indirect
464 calorimetry using CLAMS (Columbus Instruments) for 10-12 week old male mice. Mice were
465 allowed to acclimatise to the cages for two days, prior to an average of 5 days of recordings
466 being collected. Recording of body temperature and activity was carried out via surgically
467 implanted radiotelemetry devices (TA-F10, Data Sciences International). Data is shown as a
468 representative day average of single- housed age-matched males. For the diet challenge,
469 male mice were fed high-fat diet (HFD; 60% energy from fat; DIO Rodent Purified Diet, IPS
470 Ltd) for a period of 10-16 weeks from 12 weeks of age. Blood glucose was measured from tail
471 blood using the Aviva Accuchek meter (Roche). For the insulin tolerance test, mice were fasted
472 from ZT0, then injected with 0.75 IU/kg human recombinant insulin (I2643, Sigma Aldrich) at
473 ZT6 (time “0 minutes”).
474
475 **Insulin ELISA.** Insulin concentrations were measured by ELISA (EZRMI-13K Rat/Mouse
476 insulin ELISA, Merck Millipore) according to the manufacturer’s instructions. Samples were
477 diluted in matrix solution to fall within the range of the assay. Internal controls supplied with
478 the kit were run alongside the samples and were in the expected range.
479
480 **Histology.** gWAT was collected and immediately fixed in 4% paraformaldehyde for 24 hours,
481 transferred into 70% ethanol, and processed using a Leica ASP300 S tissue processor. 5μm
482 sections underwent H&E staining (Alcoholic Eosin Y solution (HT110116) and Harris
483 Haematoxylin solution (HHS16), Sigma Aldrich), Picrosirius Red staining (see below), or F4/80
484 immunohistochemistry (see below), prior to imaging using a Snapshots Olympus single slide
485 scanner at 10x or 20x objective magnification alongside Olympus cellSens Dimension

software (version 1.18). Percentage area stained was quantified using ImageJ (version 1.52a) as detailed in the online ImageJ documentation (https://imagej.nih.gov/ij/docs/examples/stained-sections/index.html), with 5-12 images quantified per animal. Adipocyte area was quantified using the Adiposoft ImageJ plug-in (version 1.16 - https://imagej.net/Adiposoft).

For Picrosirius Red staining, sections were dewaxed and rehydrated using the Leica ST5010 Autostainer XL. Sections were washed in distilled water and then transferred to Picrosirius Red (Direct Red 80, Sigma Aldrich) (without the counterstain) for 1 hour. Sections were then washed briefly in 1% acetic acid. Sections were then dehydrated, cleared and mounted using the Leica ST5010 Autostainer XL.

For F4/80 immunohistochemistry, sections were dewaxed and rehydrated prior to enzymatic antigen retrieval (trypsin from porcine pancreas (T7168, Sigma)). Sections were treated with 3% hydrogen peroxide to block endogenous peroxidase activity followed by further blocking with 5% goat serum. Rat mAb to F4/80 (1:500) (ab6640, Abcam) was added and sections were incubated overnight at 4°C. Sections were washed before addition of the biotinylated anti-rat IgG (BA-9400, H&L) secondary antibody (1:1500) for 1 hour. Sections were developed using VECTAstain® Elite® ABC kit peroxidase, followed by DAB Peroxidase substrate (Vector Labs) and counterstained with haematoxylin. Slides were then dehydrated, cleared and mounted.

Lipid extraction and gas chromatography. Total lipid was extracted from tissue lysates using chloroform-methanol (2:1; v/v) according to the Folch method (Folch et al., 1957). An internal standard (tripentadecanoin glycerol (15:0)) of known concentration of was added to samples for quantification of total triacylglyceride. Lipid fractions were separated by solid-phase extraction and fatty acid methyl esters (FAMEs) were prepared as previously described (Heath et al., 2003). Separation and detection of total triglyceride FAMEs was achieved using

a 6890N Network GC System (Agilent Technologies; CA, USA) with flame ionization detection. FAMEs were identified by their retention times compared to a standard containing 31 known fatty acids and quantified in micromolar from the peak area based on their molecular weight. The micromolar quantities were then totalled and each fatty acid was expressed as a percentage of this value (molar percentage; mol%).

Proteomics. Mice were culled by cervical dislocation and the gWAT was immediately removed and washed twice in ice-cold PBS and then once in ice-cold 0.25M sucrose, prior to samples being snap-frozen in liquid nitrogen and stored at -80°C. To extract the protein, the samples were briefly defrosted on ice and then cut into 50mg pieces and washed again in ice-cold PBS. The sample was then lysed in 200µl of 1M Triethylammonium bicarbonate buffer (TEAB; Sigma) with 0.1% (w/v) sodium dodecyl sulphate (SDS) with a Tissue Ruptor (Qiagen). Samples were centrifuged for 5 minutes, full speed, at 4°C and the supernatant collected into a clean tube. A Biorad protein assay (Biorad) was used to quantify the protein and Coomassie protein stain (InstantBlue™ Protein Stain Instant Blue, Expedeon) to check the quality of extraction. Full methods of subsequent iTRAQ proteomic analysis including bioinformatic analysis has been published previously (Xu et al., 2019). Here the raw data was searched against the mouse Swissprot database (release October 2017) using the paragon algorithm on Protein-Pilot (Version 5.0.1, AB SCIEX). A total of 33847 proteins were searched. As described (Xu et al., 2019), Bayesian protein-level differential quantification was performed by Andrew Dowsey (University of Bristol) using their own BayesProt (version 1.0.0), with default choice of priors and MCMC settings. Expression fold change relative to the control groups were determined and proteins with a global false discovery rate of >0.05 were deemed significant.

3T3-L1 cells. 3T3-L1 cells (ATCC) were maintained in Dulbecco's Modified Eagle's Medium - high glucose (DMEM/D6429, Sigma-Aldrich) supplemented with 10% Foetal Bovine Serum and 1% penicillin/streptomycin at 37°C/5% CO2. Cells were grown until confluent, passaged

and plated into 12-well tissue culture plates for differentiation. The differentiation protocol was initiated 5 days later. Cells were treated with 10µg/mL insulin (Sigma-Aldrich), 1µM dexamethasone (Sigma-Aldrich), 1µM rosiglitazone (AdooQ Bioscience) and 0.5mM IBMX (Sigma-Aldrich) prepared in DMEM + 10% FBS + 1% Pen/Strep for 3 days. On day 3 and day 5 the cell culture media was changed to 10µg/mL insulin and 1µM rosiglitazone in DMEM + 10% FBS + 1% Pen/Strep. On day 7, the cell culture media was changed to 10µg/mL insulin in DMEM + 10% FBS + 1% Pen/Strep. Finally on day 10, the cell culture media was changed to DMEM + 10% FBS + 1% Pen/Strep without any additional differentiation mediators. Cells were used from day 11 onwards. Lipid droplets were visible by day 5.

For knockdown studies, mature 3T3-L1 adipocytes were transfected with Sicontrol (Control ON-TARGETplus siRNA, Dharmacon), SiReverbα (Mouse NR1D1 ON-TARGETplus siRNA, Dharmacon) or SiReverbβ (Mouse NR1D2 ON-TARGETplus siRNA, Dharmacon) at 50nM concentration using Lipofectamine RNAiMAX (Invitrogen) as a transfection reagent. Briefly, 12-well plates were coated with poly-L-lysine hydrobromide (Sigma) and incubated for 20-30 minutes prior to excess poly-L-lysine being removed and the plates allowed to dry. SiRNAs and RNAiMAX transfection reagent were separately mixed with reduced serum media (Opti-MEM, Gibco). The control or Reverbα/β SiRNA was then added to each well and mixed with an equal quantity of RNAiMAX and then incubated for 5 minutes at room temperature. Mature 3T3-L1 adipocytes were trypsinised (trypsin-EDTA solution, Sigma) and resuspended in FBS without P/S prior to being re-plated into the wells containing the SiRNA. After 24 hours the transfection mix was removed and replaced with DMEM without FBS or P/S. The cells were then collected 48 hours after transfection.

RNA extraction (cells). RNA was extracted from cells using the ReliaPrep™ RNA Cell Miniprep system (Promega, UK), following manufacturer's instructions. RNA concentration and quality was determined with the use of a NanoDrop spectrophotometer and then stored at -80°C.

RNA extraction (tissue). Frozen adipose tissue was homogenised in TRIzol Reagent (Invitrogen) using Lysing Matrix D tubes (MP Biomedicals) and total RNA extracted according to the manufacturer's TRIzol protocol. To remove excess lipid, samples then underwent an additional centrifugation (full speed, 5 minutes, room temperature) prior to chloroform addition. For the RNA sequencing samples the isopropanol phase of TRIzol extraction was transferred to Reliaprep tissue Miniprep kit (Promega, USA) columns to ensure high quality RNA samples were used. The column was then washed, DNAse treated and RNA eluted as per protocol. RNA concentration and quality was determined with the use of a NanoDrop spectrophotometer and then stored at -80°C. For RNA-seq, RNA was diluted to 1000ng in nuclease-free water to a final volume of 20uL.

RT-qPCR. For RT-qPCR, samples were DNase treated (RQ1 RNase-Free DNase, Promega, USA) prior to cDNA conversion High Capacity RNA-to-cDNA kit (Applied Biosystems). qPCR was performed using a GoTaq qPCR Master Mix (Promega, USA) and primers listed in Supplementary Table 1 using a Step One Plus (Applied Biosystems) qPCR machine. Relative quantities of gene expression were determined using the [delta][delta] Ct method and normalised with the use of a geometric mean of the housekeeping genes *Hprt, Ppib* and *Actb*. The fold difference of expression was calculated relative to the values of control groups.

RNA-seq. Adipose tissue was collected from adult male mice (n=6-8 per group) at ZT8 and flash-frozen. Total RNA was extracted and DNase-treated as described above. Biological replicates were taken forward individually to library preparation and sequencing. For library preparation, total RNA was submitted to the Genomic Technologies Core Facility (GTCF). Quality and integrity of the RNA samples were assessed using a 2200 TapeStation (Agilent Technologies) and then libraries generated using the TruSeq® Stranded mRNA assay (Illumina, Inc.) according to the manufacturer's protocol. Briefly, total RNA (0.1-4µg) was used as input material from which polyadenylated mRNA was purified using poly-T, oligo-attached,

598 magnetic beads. The mRNA was then fragmented using divalent cations under elevated
599 temperature and then reverse transcribed into first strand cDNA using random primers.
600 Second strand cDNA was then synthesised using DNA Polymerase I and RNase H. Following
601 a single 'A' base addition, adapters were ligated to the cDNA fragments, and the products then
602 purified and enriched by PCR to create the final cDNA library. Adapter indices were used to
603 multiplex libraries, which were pooled prior to cluster generation using a cBot instrument. The
604 loaded flow-cell was then paired-end sequenced (76 + 76 cycles, plus indices) on an Illumina
605 HiSeq4000 instrument. Finally, the output data was demultiplexed (allowing one mismatch)
606 and BCL-to-Fastq conversion performed using Illumina's bcl2fastq software, version 2.17.1.14
607
608 **RNA-seq data processing & differential gene expression analysis.** Paired-end RNA-seq
609 reads were quality assessed using FastQC (v 0.11.3), FastQ Screen (v 0.9.2) (Wingett and
610 Andrews, 2018). Reads were processed with Trimmomatic (v 0.36) (Bolger et al., 2014) to
611 remove any remaining sequencing adapters and poor quality bases. RNA-seq reads were
612 then mapped against the reference genome (mm10) using STAR (version 2.5.3a) (Dobin et
613 al., 2013). Counts per gene (exons) were calculated by STAR using the genome annotation
614 from GENCODEM16. Differential expression analysis was then performed with edgeR
615 (Robinson et al., 2010) using QLF-tests based on published code (Chen et al., 2016). Changes
616 were considered significant if they reached a FDR cut-off of <0.05. Interaction analysis was
617 performed with stageR (Van den Berge et al., 2017) in conjunction with Limma voom (Law et
618 al., 2014), setting alpha at 0.05.
619
620 **Published ChIP-seq.** Raw gWAT ChIP-seq data (Zhang et al., 2015) was downloaded from
621 the GEO Sequence Read Archive (GSE67973) using the sratoolkit package (v2.9.2) (*fastq-*
622 *dump* tool). The following datasets were used: REVERBα ZT10 ChIP-seq (two replicates) -
623 SRR1977510, SRR1977511 – and ZT10 input raw data - SRR1977512. Reads were aligned
624 to the mm10 genome with Bowtie2 (v.2.3.4.3) (Langmead and Salzberg, 2012), then sorted,
625 indexed BAM files were produced with SAMtools (v.1.9) (Li et al., 2009). MACS2 (Zhang et

al., 2008) was used to call peaks from the experimental BAM files (-t) against the input control BAM file (-c), with the following options specified: *-f BAMPE -g mm --keep-dup=1 -q 0.01 --bdg --SPMR --verbose 0*. High-stringency peaks were defined as those with >7.5 fold-enrichment over input.

Integrating RNA-seq and ChIP-seq. In order to calculate enrichment of RNA-seq-based gene clusters with respect to ChIP-seq peaks, we used our in-house custom tool (Yang et al., 2019) which calculates gene cluster enrichment within specified distances from the centre of peaks (see also *Code Availability* statement below). The tool extends peaks in both directions for the given distances and extracts all genes whose TSSs overlap with the extended peaks. Given these genes, the inputted RNA-seq-based gene cluster, and the overlap of these two groups, it performs a hypergeometric test with the total number of genes in the mm10 genomes as background.

Pathway analysis. Pathway enrichment analysis of ENTREZ gene identifiers, either extracted from RNA-seq or proteomics data, was carried out using the R Bioconductor package *ReactomePA* (Yu and He, 2016). The *enrichPathway* tool was used with the following parameters: *organism = "mouse", pAdjustMethod = "BH", maxGSSize = 2000, readable = FALSE.* We considered pathways with a Padj<0.01 to be significantly enriched. For Figure S3A, no pathways had Padj<0.01 (likely due to the small number of inputted genes), hence we show the 5 pathways with the smallest Padj values.

Protein extraction and Western blotting. Small pieces (<100mg) of tissue were homogenised with the FastPrep Lysing Matrix D system (MP Biomedicals) in T-PER (Thermo Fisher Scientific), supplemented with protease inhibitor cocktail (Promega) at 1:50 dilution. Benzonase nuclease (EMD Millipore) was added (2µl), the homogenate briefly vortexed, then incubated on ice for 10 minutes. Homogenates were then centrifuged for 8 minutes at 10,000g, at 4˚C, and the supernatant removed (avoiding any lipid layer). Protein concentration was

quantified using the Bio-Rad Protein Assay (Bio-Rad). For Western blotting, equal quantities (75µg for detection of REVERBα) of protein were added to 4x NuPAGE LDS sample buffer (Invitrogen), NuPAGE sample reducing agent (dithiothreitol) (Invitrogen) and water, and denatured at 70˚C for 10 minutes. Samples were run on 4-20% Mini-PROTEAN TGX Precast Protein Gels (Bio-Rad) before wet transfer to nitrocellulose membranes. Membranes were blocked with Protein-Free Blot Blocking Buffer (Azure Biosystems), and subsequent incubation and wash steps carried out following manufacturer's instructions. Primary and secondary antibodies used were as listed in Supplementary Table 2, with primary antibodies being used at a 1:1000 dilution and secondary antibodies at 1:10,000. Membranes were imaged using chemiluminescence or the LI-COR Odyssey system. Uncropped blot images can be provided by the corresponding author upon request.

Statistics. To compare two or more groups, t-tests or ANOVAs were carried out using GraphPad Prism (v.8.4.0). For all of these, the exact statistical test used and n numbers are indicated in the figure legends. All n numbers refer to individual biological replicates (ie. individual animals). Unless otherwise specified, bar height is at mean, with error bars indicating +/-SEM. In these tests, significance is defined as *P<0.05 or **P<0.01 (P values below 0.01 were not categorised separately, i.e. no more than two stars were used, as we deemed this to be a meaningful significance cut-off). Statistical analyses of proteomics, RNA-seq and ChIP-seq data were carried out as described above in Methods, using the significance cut-offs mentioned. Plots were produced using GraphPad Prism or R package ggplot2.

Data availability. RNA-seq data generated in the course of this study has been uploaded to ArrayExpress and is available at http://www.ebi.ac.uk/arrayexpress/experiments/E-MTAB-8840. Raw proteomics data has been uploaded to Mendeley Data (https://data.mendeley.com/datasets/wskyz3rhsg/draft?a=ef40a1ec-36a4-4509-979d-32d494b96585). Other data supporting the findings of this study are available from the corresponding author upon reasonable request.

682

683 **Code availability.** The custom Python code (Yang et al., 2019) used to carry out the peaks-
684 genes enrichment analysis in this study is available at
685 http://bartzabel.ls.manchester.ac.uk//Pete/PF5HZns0zv/pegs-0.2.0.tgz.

686

ACKNOWLEDGEMENTS & AUTHOR CONTRIBUTIONS

Acknowledgements: We thank Rachel Scholey, I-Hsuan Lin, Ping Wang and Peter Briggs (Bioinformatics Core Facility, UoM), and Thea Danby (Faculty of Biology, Medicine and Health, UoM) for statistical and technical assistance, and acknowledge support of core facilities at the University of Manchester: Genomic Technologies Core Facility, Biological Services Unit, and Histological Services Unit. We also acknowledge and thank the support of our funders: the BBSRC (BB/I018654/1 to D.A.B.), the MRC (Clinical Research Training Fellowship MR/N021479/1 to A.L.H.; MR/P00279X/1 to D.A.B; MR/P011853/1 and MR/P023576/1 to D.W.R.), and the Wellcome Trust (107849/Z/15/Z, 107851/Z/15/Z).

Author Contributions: Conceptualisation, A.L.H., C.E.P., D.W.R., D.A.B.; Methodology, A.A., R.D.U., D.W.R., D.A.B.; Software, M.I., A.L.H.; Investigation, A.L.H., C.E.P., P.D., T.C., P.S.C., N.J.B., R.C.N.; Formal Analysis, A.L.H., C.E.P., R.D.U., L.H., M.I., D.A.B.; Writing, A.L.H., C.E.P., A.S.I.L., D.W.R., D.A.B.; Funding Acquisition, A.L.H., D.W.R., D.A.B.; Supervision, D.A.B.

Declaration of Interests: The authors declare no competing interests.

703 **REFERENCES**

704

705 Aucouturier J, Duché P, Timmons BW. 2011. Metabolic flexibility and obesity in children and
706 youth. *Obes Rev* **12**:e44–e53. doi:10.1111/j.1467-789X.2010.00812.x
707 Barnea M, Chapnik N, Genzer Y, Froy O. 2015. The circadian clock machinery controls
708 adiponectin expression. *Mol Cell Endocrinol* **399**:284–287.
709 doi:10.1016/j.mce.2014.10.018
710 Bass J, Takahashi JS. 2010. Circadian integration of metabolism and energetics. *Science*
711 *(80-)*. doi:10.1126/science.1195027
712 Begaye B, Vinales KL, Hollstein T, Ando T, Walter M, Bogardus C, Krakoff J, Piaggi P. 2020.
713 Impaired metabolic flexibility to high-fat overfeeding predicts future weight gain in
714 healthy adults. *Diabetes* **69**:181–192. doi:10.2337/db19-0719
715 Bolger AM, Lohse M, Usadel B. 2014. Trimmomatic: a flexible trimmer for Illumina sequence
716 data. *Bioinformatics* **30**:2114–2120. doi:10.1093/bioinformatics/btu170
717 Broussard JL, Cauter E Van. 2016. Disturbances of sleep and circadian rhythms: Novel risk
718 factors for obesity. *Curr Opin Endocrinol Diabetes Obes*.
719 doi:10.1097/MED.0000000000000276
720 Bugge A, Feng D, Everett LJ, Briggs ER, Mullican SE, Wang F, Jager J, Lazar MA. 2012.
721 Rev-erbalpha and Rev-erbbeta coordinately protect the circadian clock and normal
722 metabolic function. *Genes Dev* **26**:657–667. doi:10.1101/gad.186858.112
723 Chang J, Garva R, Pickard A, Yeung CYC, Mallikarjun V, Swift J, Holmes DF, Calverley B, Lu
724 Y, Adamson A, Raymond-Hayling H, Jensen O, Shearer T, Meng QJ, Kadler KE. 2020.
725 Circadian control of the secretory pathway maintains collagen homeostasis. *Nat Cell*
726 *Biol* **22**:74–86. doi:10.1038/s41556-019-0441-z
727 Chawla A, Lazar MA. 1993. Induction of Rev-ErbAα, an orphan receptor encoded on the
728 opposite strand of the α-thyroid hormone receptor gene, during adipocyte
729 differentiation. *J Biol Chem* **268**:16265–16269.
730 Chen Y, Lun ATL, Smyth GK. 2016. From reads to genes to pathways: differential expression

analysis of RNA-Seq experiments using Rsubread and the edgeR quasi-likelihood pipeline. *F1000Research* **5**:1438. doi:10.12688/f1000research.8987.2

Damiola F, Le Minli N, Preitner N, Kornmann B, Fleury-Olela F, Schibler U. 2000. Restricted feeding uncouples circadian oscillators in peripheral tissues from the central pacemaker in the suprachiasmatic nucleus. *Genes Dev* **14**:2950–2961. doi:10.1101/gad.183500

Delezie J, Dumont S, Dardente H, Oudart H, Grechez-Cassiau A, Klosen P, Teboul M, Delaunay F, Pevet P, Challet E. 2012. The nuclear receptor REV-ERBalpha is required for the daily balance of carbohydrate and lipid metabolism. *FASEB J* **26**:3321–3335. doi:10.1096/fj.12-208751

Dibner C, Schibler U, Albrecht U. 2010. The Mammalian Circadian Timing System: Organization and Coordination of Central and Peripheral Clocks. *Annu Rev Physiol* **72**:517–549. doi:10.1146/annurev-physiol-021909-135821

Dierickx P, Emmett MJ, Jiang C, Uehara K, Liu M, Adlanmerini M, Lazar MA. 2019. SR9009 has REV-ERB–independent effects on cell proliferation and metabolism. *Proc Natl Acad Sci* **116**:12147–12152. doi:10.1073/pnas.1904226116

Dobin A, Davis CA, Schlesinger F, Drenkow J, Zaleski C, Jha S, Batut P, Chaisson M, Gingeras TR. 2013. STAR: ultrafast universal RNA-seq aligner. *Bioinformatics* **29**:15–21. doi:10.1093/bioinformatics/bts635

Dudek M, Gossan N, Yang N, Im H-J, Ruckshanthi JPD, Yoshitane H, Li X, Jin D, Wang P, Boudiffa M, Bellantuono I, Fukada Y, Boot-Handford RP, Meng Q-J. 2015. The chondrocyte clock gene Bmal1 controls cartilage homeostasis and integrity. *J Clin Invest* **126**:365–376. doi:10.1172/JCI82755

Dyar KA, Lutter D, Artati A, Ceglia NJ, Liu Y, Armenta D, Jastroch M, Schneider S, de Mateo S, Cervantes M, Abbondante S, Tognini P, Orozco-Solis R, Kinouchi K, Wang C, Swerdloff R, Nadeef S, Masri S, Magistretti P, Orlando V, Borrelli E, Uhlenhaut NH, Baldi P, Adamski J, Tschöp MH, Eckel-Mahan K, Sassone-Corsi P. 2018. Atlas of Circadian Metabolism Reveals System-wide Coordination and Communication between Clocks. *Cell* **174**:1571-1585.e11. doi:10.1016/j.cell.2018.08.042

759 Eckel-Mahan KL, Patel VR, De Mateo S, Orozco-Solis R, Ceglia NJ, Sahar S, Dilag-Penilla
760 SA, Dyar KA, Baldi P, Sassone-Corsi P. 2013. Reprogramming of the circadian clock by
761 nutritional challenge. *Cell* **155**:1464–1478. doi:10.1016/j.cell.2013.11.034
762 Eguchi J, Wang X, Yu S, Kershaw EE, Chiu PC, Dushay J, Estall JL, Klein U, Maratos-Flier
763 E, Rosen ED. 2011. Transcriptional Control of Adipose Lipid Handling by IRF4. *Cell*
764 *Metab* **13**:249–259. doi:10.1016/j.cmet.2011.02.005
765 Feng D, Liu T, Sun Z, Bugge A, Mullican SE, Alenghat T, Liu XS, Lazar MA. 2011. A circadian
766 rhythm orchestrated by histone deacetylase 3 controls hepatic lipid metabolism.
767 *Science (80-)* **331**:1315–1319. doi:10.1126/science.1198125
768 Folch J, Lees M, Sloane Stanley GH. 1957. A simple method for the isolation and purification
769 of total lipides from animal tissues. *J Biol Chem* **226**:497–509.
770 Gerhart-Hines Z, Feng D, Emmett MJ, Everett LJ, Loro E, Briggs ER, Bugge A, Hou C,
771 Ferrara C, Seale P, Pryma DA, Khurana TS, Lazar MA. 2013. The nuclear receptor
772 Rev-erbα controls circadian thermogenic plasticity. *Nature* **503**:410–413.
773 doi:10.1038/nature12642
774 Goldstein I, Baek S, Presman DM, Paakinaho V, Swinstead EE, Hager GL. 2017.
775 Transcription factor assisted loading and enhancer dynamics dictate the hepatic fasting
776 response. *Genome Res* **27**:427–439. doi:10.1101/gr.212175.116
777 Guan D, Xiong Y, Borck PC, Jang C, Doulias P-T, Papazyan R, Fang B, Jiang C, Zhang Y,
778 Briggs ER, Hu W, Steger D, Ischiropoulos H, Rabinowitz JD, Lazar MA. 2018. Diet-
779 Induced Circadian Enhancer Remodeling Synchronizes Opposing Hepatic Lipid
780 Metabolic Processes. *Cell* **174**:831-842.e12. doi:10.1016/j.cell.2018.06.031
781 Guo H, Brewer JM, Champhekar A, Harris RBS, Bittman EL. 2005. Differential control of
782 peripheral circadian rhythms by suprachiasmatic-dependent neural signals. *Proc Natl*
783 *Acad Sci* **102**:3111–3116. doi:10.1073/pnas.0409734102
784 Hand LE, Usan P, Cooper GJS, Xu LY, Ammori B, Cunningham PS, Aghamohammadzadeh
785 R, Soran H, Greenstein A, Loudon ASI, Bechtold DA, Ray DW. 2015. Adiponectin
786 Induces A20 Expression in Adipose Tissue to Confer Metabolic Benefit. *Diabetes*

64:128–136. doi:10.2337/db13-1835

Heath RB, Karpe F, Milne RW, Burdge GC, Wootton SA, Frayn KN. 2003. Selective partitioning of dietary fatty acids into the VLDL TG pool in the early postprandial period. *J Lipid Res* **44**:2065–2072. doi:10.1194/jlr.M300167-JLR200

Hughes ME, Hong H-K, Chong JL, Indacochea AA, Lee SS, Han M, Takahashi JS, Hogenesch JB. 2012. Brain-specific rescue of Clock reveals system-driven transcriptional rhythms in peripheral tissue. *PLoS Genet* **8**:e1002835. doi:10.1371/journal.pgen.1002835

Hunter AL, Pelekanou CE, Adamson A, Downton P, Barron NJ, Cornfield T, Poolman TM, Humphreys N, Cunningham PS, Hodson L, Loudon AS, Iqbal M, Bechtold DA, Ray DW. 2020. Nuclear receptor REVERBα is a state-dependent regulator of liver energy metabolism. *Proc Natl Acad Sci U S A* **In press**. doi:10.1073/pnas.2005330117

Jager J, Wang F, Fang B, Lim H-W, Peed LC, Steger DJ, Won K-J, Kharitonenkov A, Adams AC, Lazar MA. 2016. The Nuclear Receptor Rev-erbα Regulates Adipose Tissue-specific FGF21 Signaling. *J Biol Chem* **291**:10867–75. doi:10.1074/jbc.M116.719120

Jeffery E, Berry R, Church CD, Yu S, Shook BA, Horsley V, Rosen ED, Rodeheffer MS. 2014. Characterization of Cre recombinase models for the study of adipose tissue. *Adipocyte* **3**:206–211. doi:10.4161/adip.29674

Jonker JW, Suh JM, Atkins AR, Ahmadian M, Li P, Whyte J, He M, Juguilon H, Yin YQ, Phillips CT, Yu RT, Olefsky JM, Henry RR, Downes M, Evans RM. 2012. A PPARγ-FGF1 axis is required for adaptive adipose remodelling and metabolic homeostasis. *Nature* **485**:391–394. doi:10.1038/nature10998

Kim HJ, Choi S, Kim Kyuwoong, Park H, Kim Kyae-hyung, Park SM, Jun H, Choi S, Kim Kyuwoong, Park H, Kim HJ. 2019. Association between misalignment of circadian rhythm and obesity in Korean men : Sixth Korea National Health and Nutrition Examination Survey Association between misalignment of circadian rhythm and obesity in Korean men : Sixth Korea National Health and . *Chronobiol Int* **00**:1–9. doi:10.1080/07420528.2019.1671439

815 Kim JY, Van De Wall E, Laplante M, Azzara A, Trujillo ME, Hofmann SM, Schraw T, Durand
816 JL, Li H, Li G, Jelicks LA, Mehler MF, Hui DY, Deshaies Y, Shulman GI, Schwartz GJ,
817 Scherer PE. 2007. Obesity-associated improvements in metabolic profile through
818 expansion of adipose tissue. *J Clin Invest* **117**:2621–2637. doi:10.1172/JCI31021
819 Kim YH, Marhon SA, Zhang Y, Steger DJ, Won KJ, Lazar MA. 2018. Rev-erba dynamically
820 modulates chromatin looping to control circadian gene transcription. *Science (80-)*
821 **359**:1274–1277. doi:10.1126/science.aao6891
822 Kinouchi K, Magnan C, Ceglia N, Liu Y, Cervantes M, Pastore N, Huynh T, Ballabio A, Baldi
823 P, Masri S, Sassone-Corsi P. 2018. Fasting Imparts a Switch to Alternative Daily
824 Pathways in Liver and Muscle. *Cell Rep* **25**:3299-3314.e6.
825 doi:10.1016/j.celrep.2018.11.077
826 Kolbe I, Husse J, Salinas G, Lingner T, Astiz M, Oster H. 2016. The SCN Clock Governs
827 Circadian Transcription Rhythms in Murine Epididymal White Adipose Tissue. *J Biol*
828 *Rhythms* **31**:577–587. doi:10.1177/0748730416666170
829 Kornmann B, Schaad O, Bujard H, Takahashi JS, Schibler U. 2007. System-driven and
830 oscillator-dependent circadian transcription in mice with a conditionally active liver
831 clock. *PLoS Biol* **5**:e34. doi:10.1371/journal.pbio.0050034
832 Koronowski KB, Kinouchi K, Welz PS, Smith JG, Zinna VM, Shi J, Samad M, Chen S,
833 Magnan CN, Kinchen JM, Li W, Baldi P, Benitah SA, Sassone-Corsi P. 2019. Defining
834 the Independence of the Liver Circadian Clock. *Cell* **177**:1448–1462.
835 doi:10.1016/j.cell.2019.04.025
836 Kumar N, Solt LA, Wang Y, Rogers PM, Bhattacharyya G, Kamenecka TM, Stayrook KR,
837 Crumbley C, Floyd ZE, Gimble JM, Griffin PR, Burris TP. 2010. Regulation of
838 adipogenesis by natural and synthetic REV-ERB ligands. *Endocrinology* **151**:3015–
839 3025. doi:10.1210/en.2009-0800
840 Lamia KA, Storch K-F, Weitz CJ. 2008. Physiological significance of a peripheral tissue
841 circadian clock. *Proc Natl Acad Sci* **105**:15172–7. doi:10.1073/pnas.0806717105
842 Langmead B, Salzberg SL. 2012. Fast gapped-read alignment with Bowtie 2. *Nat Methods*

9:357–359. doi:10.1038/nmeth.1923

Law CW, Chen Y, Shi W, Smyth GK. 2014. voom: Precision weights unlock linear model analysis tools for RNA-seq read counts. *Genome Biol* **15**:R29. doi:10.1186/gb-2014-15-2-r29

Le Martelot G, Claudel T, Gatfield D, Schaad O, Kornmann B, Lo Sasso G, Moschetta A, Schibler U. 2009. REV-ERBα participates in circadian SREBP signaling and bile acid homeostasis. *PLoS Biol* **7**:e1000181. doi:10.1371/journal.pbio.1000181

Li H, Handsaker B, Wysoker A, Fennell T, Ruan J, Homer N, Marth G, Abecasis G, Durbin R, 1000 Genome Project Data Processing Subgroup. 2009. The Sequence Alignment/Map format and SAMtools. *Bioinformatics* **25**:2078–2079. doi:10.1093/bioinformatics/btp352

Masri S, Papagiannakopoulos T, Kinouchi K, Liu Y, Cervantes M, Baldi P, Jacks T, Sassone-Corsi P. 2016. Lung Adenocarcinoma Distally Rewires Hepatic Circadian Homeostasis. *Cell* **165**:896–909. doi:10.1016/j.cell.2016.04.039

Mistlberger RE. 1994. Circadian food-anticipatory activity: formal models and physiological mechanisms. *Neurosci Biobehav Rev* **18**:171–95.

Paschos GK, Ibrahim S, Song W-LL, Kunieda T, Grant G, Reyes TM, Bradfield CA, Vaughan CH, Eiden M, Masoodi M, Griffin JL, Wang F, Lawson JA, Fitzgerald GA. 2012. Obesity in mice with adipocyte-specific deletion of clock component Arntl. *Nat Med* **18**:1768–1777. doi:10.1038/nm.2979

Preitner N, Damiola F, Luis-Lopez-Molina, Zakany J, Duboule D, Albrecht U, Schibler U. 2002. The Orphan Nuclear Receptor REV-ERBα Controls Circadian Transcription within the Positive Limb of the Mammalian Circadian Oscillator. *Cell* **110**:251–260. doi:10.1016/S0092-8674(02)00825-5

Quagliarini F, Mir AA, Balazs K, Wierer M, Dyar KA, Jouffe C, Makris K, Hawe J, Heinig M, Filipp FV, Barish GD, Uhlenhaut NH. 2019. Cistromic Reprogramming of the Diurnal Glucocorticoid Hormone Response by High-Fat Diet. *Mol Cell* **76**:531-545.e5. doi:10.1016/j.molcel.2019.10.007

Reinke H, Asher G. 2019. Crosstalk between metabolism and circadian clocks. *Nat Rev Mol*

Cell Biol. doi:10.1038/s41580-018-0096-9

Robinson MD, McCarthy DJ, Smyth GK. 2010. edgeR: a Bioconductor package for differential expression analysis of digital gene expression data. *Bioinformatics* **26**:139–140. doi:10.1093/bioinformatics/btp616

Sherratt MJ, Hopkinson L, Naven M, Hibbert SA, Ozols M, Eckersley A, Newton VL, Bell M, Meng Q-J. 2019. Circadian rhythms in skin and other elastic tissues. *Matrix Biol*. doi:10.1016/j.matbio.2019.08.004

Shostak A, Meyer-Kovac J, Oster H. 2013. Circadian regulation of lipid mobilization in white adipose tissues. *Diabetes* **62**:2195–2203. doi:10.2337/db12-1449

Solt LA, Wang Y, Banerjee S, Hughes T, Kojetin DJ, Lundasen T, Shin Y, Liu J, Cameron MD, Noel R, Yoo S-H, Takahashi JS, Butler AA, Kamenecka TM, Burris TP. 2012. Regulation of circadian behaviour and metabolism by synthetic REV-ERB agonists. *Nature* **485**:62–8. doi:10.1038/nature11030

Tognini P, Murakami M, Liu Y, Eckel-Mahan KL, Newman JC, Verdin E, Baldi P, Sassone-Corsi P. 2017. Distinct Circadian Signatures in Liver and Gut Clocks Revealed by Ketogenic Diet. *Cell Metab* **26**:523-538.e5. doi:10.1016/j.cmet.2017.08.015

Van den Berge K, Soneson C, Robinson MD, Clement L. 2017. stageR: A general stage-wise method for controlling the gene-level false discovery rate in differential expression and differential transcript usage. *Genome Biol* **18**:151. doi:10.1186/s13059-017-1277-0

Virtue S, Petkevicius K, Moreno-Navarrete JM, Jenkins B, Hart D, Dale M, Koulman A, Fernández-Real JM, Vidal-Puig A. 2018. Peroxisome Proliferator-Activated Receptor γ2 Controls the Rate of Adipose Tissue Lipid Storage and Determines Metabolic Flexibility. *Cell Rep* **24**:2005-2012.e7. doi:10.1016/j.celrep.2018.07.063

West AC, Bechtold DA. 2015. The cost of circadian desynchrony: Evidence, insights and open questions. *BioEssays* **37**:777–788. doi:10.1002/bies.201400173

Wingett SW, Andrews S. 2018. FastQ Screen: A tool for multi-genome mapping and quality control. *F1000Research* **7**:1338. doi:10.12688/f1000research.15931.2

Xu J, Patassini S, Rustogi N, Riba-Garcia I, Hale BD, Phillips AM, Waldvogel H, Haines R,

899 Bradbury P, Stevens A, Faull RLM, Dowsey AW, Cooper GJS, Unwin RD. 2019.
900 Regional protein expression in human Alzheimer's brain correlates with disease
901 severity. *Commun Biol* **2**:43. doi:10.1038/s42003-018-0254-9
902 Yamamoto T, Nakahata Y, Soma H, Akashi M, Mamine T, Takumi T. 2004. Transcriptional
903 oscillation of canonical clock genes in mouse peripheral tissues. *BMC Mol Biol* **5**:18.
904 doi:10.1186/1471-2199-5-18
905 Yang S-H, Andrabi M, Biss R, Baker SM, Iqbal M, Sharrocks AD. 2019. ZIC3 Controls the
906 Transition from Naïve to Primed Pluripotency. *Cell Rep* **27**:3215–3227.
907 doi:10.1016/j.celrep.2019.05.026
908 Yu G, He QY. 2016. ReactomePA: An R/Bioconductor package for reactome pathway
909 analysis and visualization. *Mol Biosyst* **12**:477–479. doi:10.1039/c5mb00663e
910 Zhang Y, Fang B, Damle M, Guan D, Li Z, Kim YH, Gannon M, Lazar MA. 2016. HNF6 and
911 Rev-erbalpha integrate hepatic lipid metabolism by overlapping and distinct
912 transcriptional mechanisms. *Genes Dev* **30**:1636–1644. doi:10.1101/gad.281972.116
913 Zhang Y, Fang B, Emmett MJ, Damle M, Sun Z, Feng D, Armour SM, Remsberg JR, Jager J,
914 Soccio RE, Steger DJ, Lazar MA. 2015. Discrete functions of nuclear receptor Rev-
915 erbalpha couple metabolism to the clock. *Science (80-)* **348**:1488–1492.
916 doi:10.1126/science.aab3021
917 Zhang Y, Liu T, Meyer CA, Eeckhoute J, Johnson DS, Bernstein BE, Nussbaum C, Myers
918 RM, Brown M, Li W, Liu XS. 2008. Model-based Analysis of ChIP-Seq (MACS).
919 *Genome Biol* **9**:R137. doi:10.1186/gb-2008-9-9-r137
920 Zhang Y, Papazyan R, Damle M, Fang B, Jager J, Feng D, Peed LC, Guan D, Sun Z, Lazar
921 MA. 2017. The hepatic circadian clock fine-tunes the lipogenic response to feeding
922 through RORα/γ. *Genes Dev* **31**:1202–1211. doi:10.1101/gad.302323.117
923

SUPPLEMENTARY TABLE 1 - **qPCR primer sequences**

Gene	Forward Primer (5'-3')	Reverse Primer (5'-3')
Acaca	TAATGGGCTGCTTCTGTGACTC	TCAATATCGCCATCACTCTTG
Acss3	AATGTCGCAAAGTAACAGGCG	GTGGGTCTTGTACTCACCACC
Actb	GGCTGTATTCCCCTCCATCG	CCAGTTGGTAACAATGCCATGT
Bmal1	GTCGAATGATTGCCGAGGAA	GGGAGGCGTACTTGTGATGTTC
Cd36	CCACAGTTGGTGTGTTTTATCC	TCAATTATGGCAACTTTGCTT
Col1a1	TCCCAGAACATCACCTATCAC	CTGTTGCCTTCGCCTCTGAG
Col5a3	TACCTCTGGTAACCGGGGTCTC	CCTTTTGGTCCCTCATCACCC
Col6a1	TGCCCTGTGGATCTATTCTTCG	CTGTCTCTCAGGTTGTCAATG
Col6a2	TGGTCAACAGGCTAGGTGCCAT	TAGACAGGGAGTTGACTCGCTC
Col6a3	CTGTCGCCTGCATTCATC	ACAACCCTCTGCACAAAGTC
Dio2	CCAGACAACTAGCATGGCGT	GAAAATTGGCTGCCCCACAC
Elovl6	GAGCAGAGGCGCAGAGAAC	ATGCCGACCACCAAAGATAA
Fasn	CCCAGAGGCTTGTGCTGACT	CGAATGTGCTTGGCTTGGT
G6pdx	AGACCTGCATGAGTCAGACG	TGGTTCGACAGTTGATTGGA
Hprt	GTTGGATACAGGCCAGACTTTGTTG	GATTCAACTTGCGCTCATCTTAGGC
Loxl4	TTGCTCTCAAGGACACCTGGTA	GCAGCGAACTCCACTCATCA
Lpl	AGGGCTCTGCCTGAGTTGTA	CCATCCTCAGTCCCAGAAAA
Me1	GGGATTGCTCACTTGGTTGT	GTTCATGGGCAAACACCTCT
Pfk1	TGCAGCCTACAATCTGCTCC	GTCAAGTGTGCGTAGTTCTGA
Plin2	AAGAGGCCAAACAAAAGAGCCAGGAGACCA	ACCCTGAATTTTCTGGTTGGCACTGTGCAT
Ppib	GGAGATGGCACAGGAGGAAA	CCGTAGTGCTTCAGTTTGAAGTTCT
Reverbα	GTCTCTCCGTTGGCATGTCT	CCAAGTTCATGGCGCTCT
Reverbβ	CAGGAGGTGTGATTGCCTACA	GGACGAGGACTGGAAGCTAAT
Scd1	CGCTGGTGCCCTGGTACTGC	CAGCCAGGTGGCGTTGAGCA
Ucp1	ACTGCCACACCTCCAGTCATT	CTTTGCCTCACTCAGGATTGG

SUPPLEMENTARY TABLE 2 – **Antibodies**

Source and target	**Manufacturer**	**Catalogue identifier, lot**	**Use**
Rabbit polyclonal anti-REVERBα (NR1D1)	ProteinTech	Cat#14506-1-AP, lot 5745; RRID:AB_11182604	Western blot, primary
Mouse monoclonal anti-UCP1 (clone 536435)	R&D Systems	Cat#MAB6158, lot CCNV0218091; RRID:AB_10572490	Western blot, primary
Mouse monoclonal anti-β-ACTIN (ACTB)	ProteinTech	Cat#60008-1, lot 0001084; RRID:AB_2289225	Western blot, primary
Sheep Anti-Mouse IgG, HRP-linked whole Ab	GE Healthcare	Cat#NA931V, lot 16908225; RRID:AB_772210	Western blot, secondary
Donkey Anti-Rabbit IgG, HRP-linked whole Ab	GE Healthcare	Cat#NA934V, lot 16921443; RRID:AB_772206	Western blot, secondary
Goat polyclonal Anti-Rabbit IgG (H+L), DyLight 680 Conjugate	Cell Signaling Technology	Cat#5366P, lot 7; RRID:AB_10693812	Western blot, secondary
Rat monoclonal anti-F4/80	Abcam	Cat#ab6640, lot 845724; RRID:AB_1140040	Immunohistochemistry, primary
Goat biotinylated anti-rat IgG (affinity purified)	H&L	Cat#BA-9400, lot ZB1216; RRID:AB_2336202	Immunohistochemistry, secondary